5.3.1 Width and Height of the Weld Bead

The width and height of the weld bead are both proportional to the square root of the heat input.[3] This result was attributed to the linear relationship between the area of bead reinforcement and the heat input.

In this work the width of the weld bead was calculated using Equation 3. The peak temperature was calculated as a function of y distance (z=0), and the bead width was found when the peak temperature became equal to the melting temperature of the substrate material. Comparisons of the calculated bead width with the experimental data of Clark, and Alberry et al. are given in Figs. 5.5a, b with the regression analysis results.

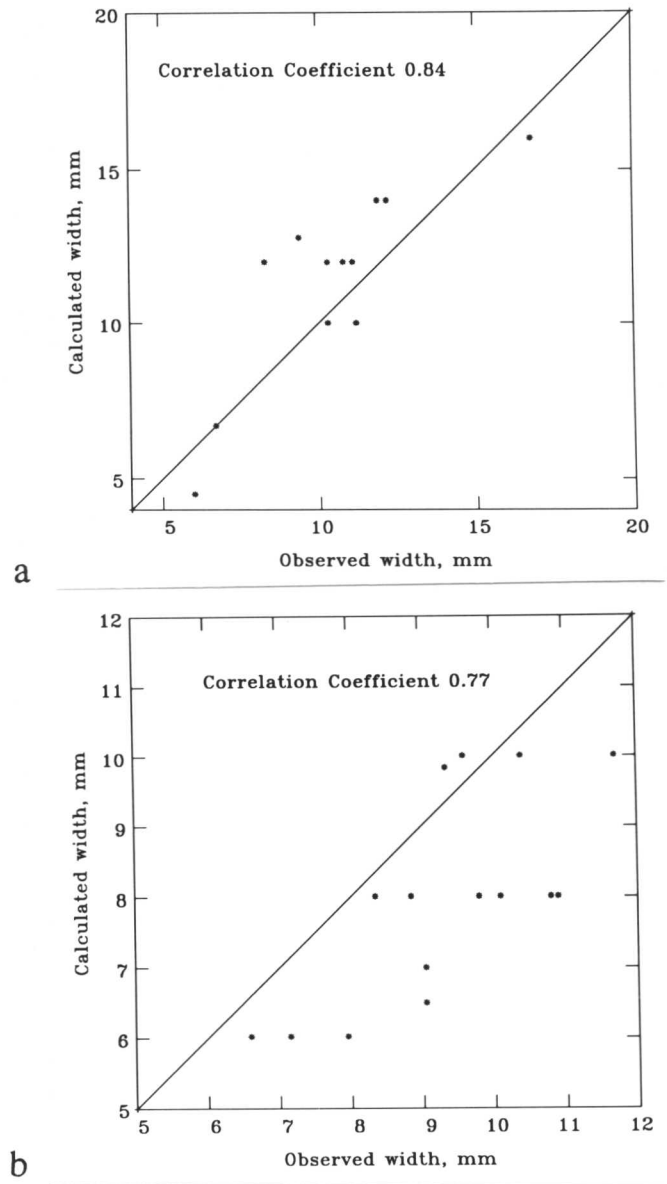

Fig. 5.5: Calculated bead width versus observed bead width a) data after Clark for the MMA deposits; b) data after Alberry et al. for the TIG deposits. During calculations r_b is assumed to be equal to the electrode diameter for the MMA, and wire diameter for the TIG, processes.

The bead height was calculated using the simple geometry of the weld bead. Assuming that the weld bead has a spherical geometry, and the bead is bounded by an arc of a circle of radius r_1, subtending at angle of 2θ for the reinforcement, the area of bead reinforcement, A_1, can be calculated as follows;

$$A_1 = \theta {r_1}^2 - \frac{1}{2}(r_1 - h)w \qquad \text{.....(8)}$$

where w is the bead width, and h is the bead height.

Defining k = w / 2h, Equation 8 may be written

$$r_1 = \frac{h^2 + \frac{1}{4}w^2}{2h} = h\left(\frac{1+k^2}{2}\right) \qquad \text{.....(9)}$$

$$\theta = \sin^{-1}\left(\frac{\frac{1}{2}w}{h^2 + \frac{1}{4}w^2)/2h}\right) = \sin^{-1}\left(\frac{w/h}{1 + \frac{1}{4}(w^2/h^2)}\right)$$

$$= \sin^{-1}\left(\frac{2k}{1+k^2}\right) \qquad \text{.....(10)}$$

so that

$$A_1 = \sin^{-1}\left(\frac{2k}{1+k^2}\right)h^2\left(\frac{1+k^2}{2}\right)^2 - h^2 k\left(\frac{k^2-1}{2}\right) \qquad \text{.....(11)}$$

Having calculated the bead width and the area of bead reinforcement, the bead height is calculated through Equation 11. This is carried out using the Newton-Raphson iteration method[6] and the results which are compared with the experimental data of Clark for the MMA deposits are given in Fig. 5.6.

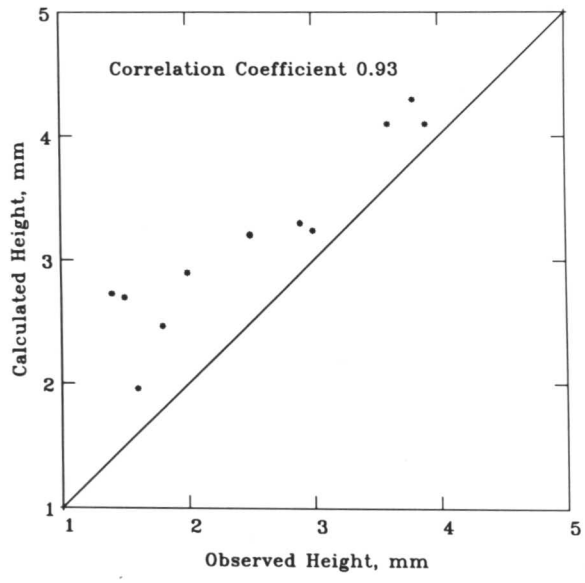

Fig. 5.6: Calculated bead height versus observed bead height, data after Clark[3] for the MMA deposits.

5.3.2 Penetration Depth

Similar to the bead width calculations, an attempt has been made to predict the penetration depth using the heat flow equations. The peak temperature is calculated below the centre of the arc (y=0) by increasing the z distance until the peak temperature becomes equal to the melting temperature of the base plate. The results are compared with the experimental data in Figs. 5.7a,b.

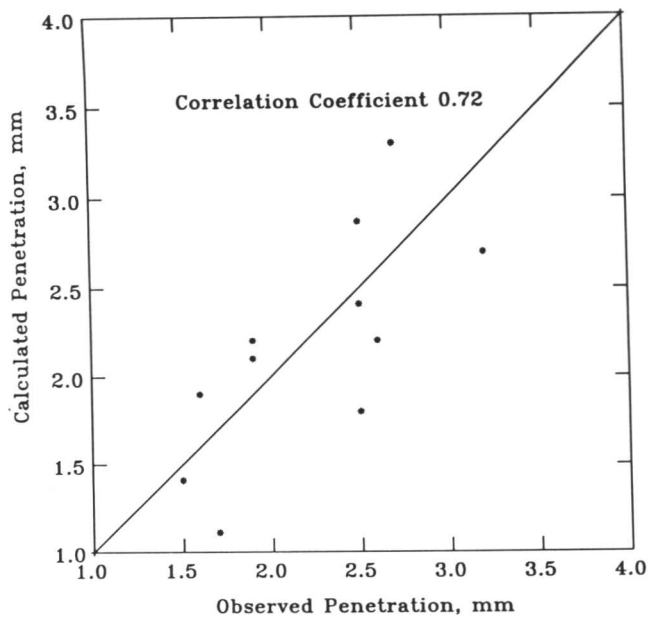

a

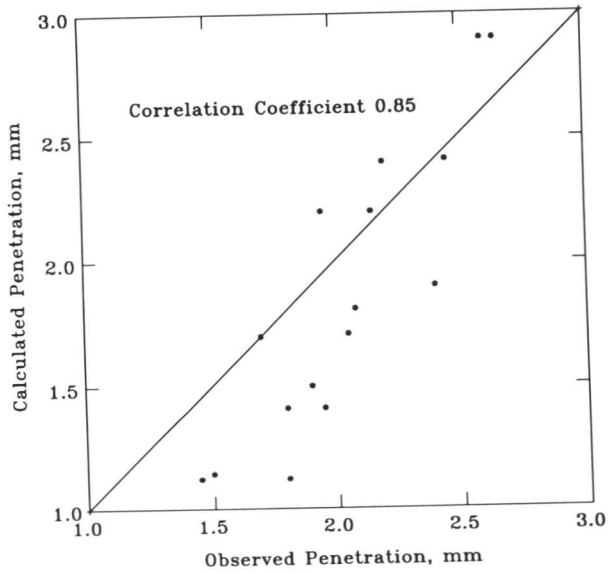

b

Fig. 5.7: Calculated penetration depth versus observed penetration depth a) data after Clark for the MMA deposits; b) data after Alberry et al. for the TIG deposits.

The results indicate that the penetration depth cannot be calculated accurately using the heat flow equations. This is not surprising since no account is taken of factors such as convective mixing in the pool, variations caused by a change in shielding gas, and flux, magnetic forces, surface heat losses, impact of fused droplets on the pool, etc. Therefore, many empirical attempts have been made to predict the penetration depth, some of them were discussed in Chapter 4.

5.3.3 Melted Area and Dilution

During welding processes, the substrate material is melted to ensure good bonding of the applied material. The total melted area depends on the welding conditions, and the melting temperature of the substrate material. The composition of the weld deposit is therefore influenced by the mixing of the base material with the deposit so that calculation of the total melted area is necessary. The melted area has been calculated similar to the area of bead reinforcement. Assuming the weld has a spherical geometry and bead is bounded by an arc of a circle of radius r_2, subtending an angle of 2θ, the total melted area is written as;

$$A_2 = \theta {r_2}^2 - \frac{1}{2}(r_2 - p)w \qquad \text{.....(12)}$$

where p is the penetration.

Defining l = h/p

$$r_2 = \frac{p^2 + \frac{1}{4}w^2}{2p} = p\left(\frac{1 + k^2l^2}{2}\right) = \frac{h}{l}\left(\frac{1 + k^2l^2}{2}\right) \qquad \text{.....(13)}$$

$$\theta = \sin^{-1}\left(\frac{2kl}{1 + k^2l^2}\right) \qquad \text{.....(14)}$$

so that

$$A_2 = \sin^{-1}\left(\frac{2kl}{1 + k^2l^2}\right)\frac{h^2}{l^2}\left(\frac{1 + k^2l^2}{2}\right)^2 - \frac{h^2k}{l}\left(\frac{k^2l^2 - 1}{2}\right) \qquad \text{.....(15)}$$

Dilution[1] is one of the important factors influencing the properties of hardfacing deposits. Therefore, calculations are compared with the experimental results of Alberry et al.[4] (Fig. 5.8). Regression analysis results showed that the correlation coefficient is ≈0.89, indicating reasonable agreement between the calculated and measured degrees of dilution.

[1] The dilution is defined in Fig. 4.1 as A_2/A_1+A_2.

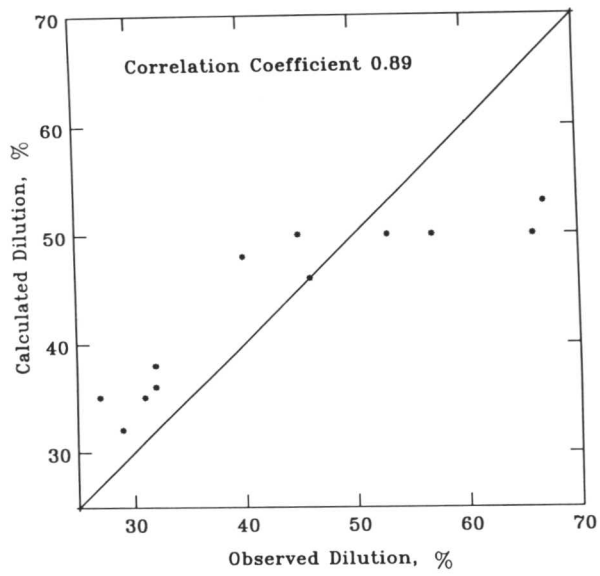

Fig. 5.8: Calculated dilution versus observed dilution. Data after Alberry et al.[4]

The welding variables in hardfacing alloys determine the level of dilution. For example, Fig. 5.9 illustrates the influence of the arc power on the dilution. It can be seen that the dilution varies from 6% to 50% when the arc power is increased to 3750J/s from 1250J/s. Furthermore, the volume fraction of microconstituents in the deposited material are influenced by the welding parameters primarily through the dilution. Carbides are the most effective phases in enhancing abrasive wear resistance and therefore their volume fraction should be optimised. The influence of the arc power on the volume fraction of M_7C_3 carbides (when the M_7C_3 carbide is in equilibrium with austenite at 1373K) in Fe-34Cr-4.5C (wt%) is illustrated in Fig. 5.10. The volume fraction of the carbides has been calculated using the thermodynamic program described in Chapter 7. The figure clearly demonstrates that the volume fraction of phases, and therefore wear resistance, can be controlled by adjusting the welding variables.

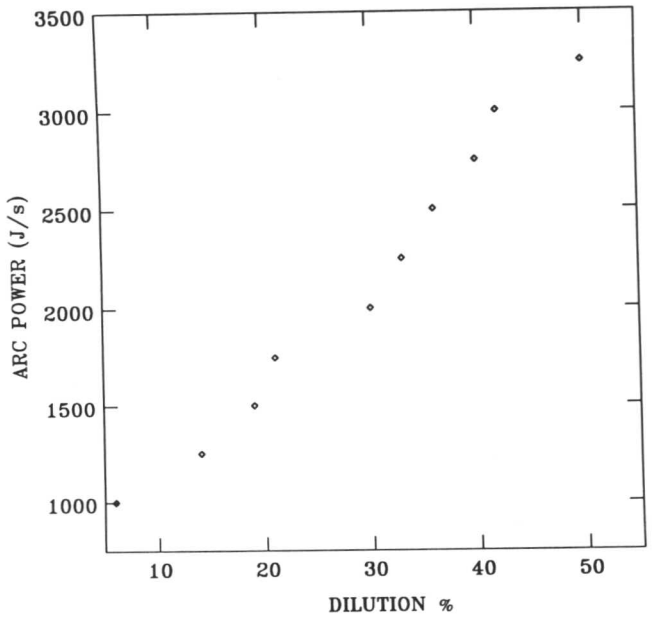

Fig. 5.9: The influence of the arc power on the dilution. The welding conditions are assumed to be q = 1500J/s, r_b = 2mm, υ= 4mm, and T_o = 293K.

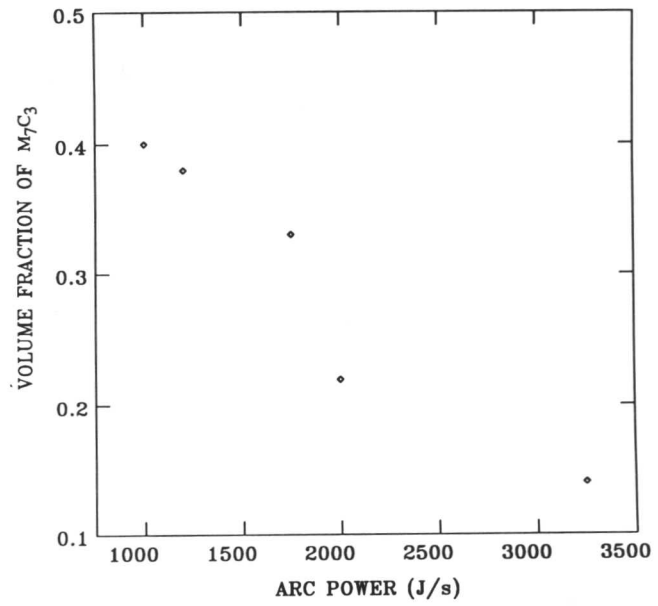

Fig. 5.10: The influence of the arc power on the volume fraction of M_7C_3 carbides in Fe-34Cr-4.5C (wt%) alloy. The volume fraction of carbides are calculated using the thermodynamic program, outlined in Chapter 7. The alloy is assumed to be configurationally frozen at 1373K. The welding conditions are; q = 1500J/s, r_b = 2mm, υ= 4mm, and T_o = 293K.

5.4 Conclusions

Three dimensional heat flow equations for a circular disc source have been used to calculate the weld bead dimensions and the degree of dilution for arc welding processes. Temperature-time profiles were computed for a given point in the weld bead so that heating and cooling rates could be calculated as a function of welding parameters. This is particularly important in hardfacing alloys since the cooling rate has an important influence on carbide precipitation, and on the morphology and composition of phases. The area of bead reinforcement, total melted area, dilution, the height and the width of the weld bead were calculated. The results obtained were compared with the data in the literature and the agreement was found to be excellent. The influence of arc power on the volume fraction of carbides was determined, and the results suggest that abrasive wear resistance of the hardfacing deposits could be optimised by adjusting the welding variables.

5.5 REFERENCES

1) D. ROSENTHAL: Trans. Am. Soc. Mech. Engnrs., 1946, **68**, 849.
2) J. C. ION, K. E. EASTERLING, and M. F. ASHBY: Acta Metall., 1984, **32**, 1949.
3) J. N. CLARK: Materials Science and Technology, 1985, **1**, Part I, 1081.
4) P. J. ALBERRY, R. R. L. BRUNNSTROM, and K. E. JONES: Metals Technology, 1983, **10**, 28.
5) M. F. ASHBY, and K. E. EASTERLING: Acta Metall., 1982, **30**, 169.
6) "Numerical Recipes", W. H. PRESS, B. P. FLANNERY, S. A. TEUKOLSKY, and W. T. VETTERLING, The Art of Scientific Computing, Cambridge University Press, 1987.

6. THE EFFECT OF MICROSTRUCTURE ON ABRASIVE WEAR RESISTANCE

6.1 Introduction

In this section the effect of microstructure on abrasive wear, oxidation, corrosion resistance and matrix stability will be examined.

6.2 Effect of Hardness

It is known that there is a significant effect of the second phases, such as precipitates, carbides and soft microstructural constituents (e.g. residual austenite) on abrasive wear resistance. The influence of hard particles on wear resistance partly depends on their hardness. Soft particles (coherent or semicoherent) are sheared by dislocations and hence, there is usually only a slight increase in wear resistance as a consequence of the presence of soft particles, especially under heavy abrasive conditions. It has been confirmed that there is no simple proportionality between abrasive wear rate and overall hardness.[1-3] In fact it is the hardness of the worn surface which is regarded as an important factor in determining abrasive wear resistance.[1-3] Fig. 6.1 shows the variations of the gouging wear ratio as a function of the hardness of the initial and of the worn surface in a wide range of ferrous alloys. It is evident from Fig. 6.1 that materials surface harden to different degrees, as evidenced by the differences in the length of the horizontal junctions between the corresponding data points. For example, austenitic stainless steels and austenitic manganese steels reveal relatively large ranges of work hardening due to their high deformation absorption capacity and in some cases due to strain-induced martensite transformation. In Fig. 6.1 the points A and B represent typical differences of the capacity to work harden between quenched and tempered steel, and Hadfield steel. Good correlation between abrasive wear resistance and the hardness of the worn surface supports the conclusion that wear resistance is a function of the maximum hardness of the work hardened surface.

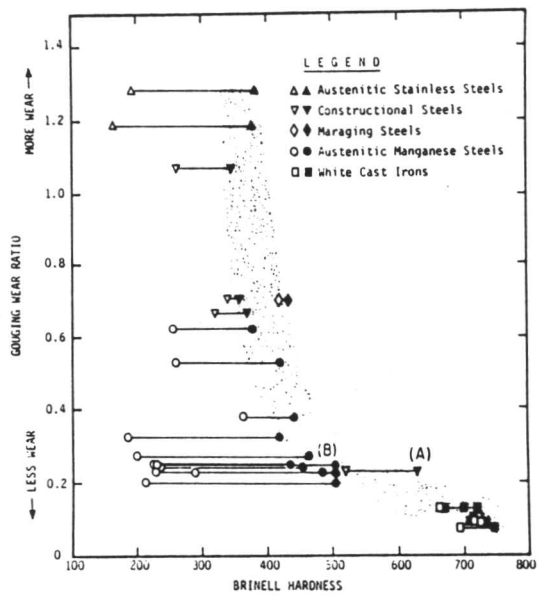

Fig. 6.1: Gouging wear ratio versus initial hardness (open points), and work-hardened hardness (full points) of a wide variety of ferrous materials.[4]

6.2.1 Effect of Carbides

Carbides are the most effective contributors to wear resistance due to their high hardness. The hardness of carbides generally depends on their crystal structure, alloying elements[5] and their concentration,[6] and as suggested by Maratray[7] and Su et al.,[5] their crystal faces. They showed that the hardness perpendicular to the long axis of the M_7C_3 carbides is considerably higher than that along their length. Although it is accepted that wear resistance increases with the hardness of the carbide particles, experimental studies have shown that wear resistance is better related to the difference between the hardness of material and that of the abrasives. If the two have a comparable hardness, the rate of material removal decreases as the -2.5th power of the alloy hardness, and when the material hardness is higher than the abrasive hardness, the rate decreases as the sixth power.[8] As seen in Fig. 6.2 the wear rate of materials increases significantly when the hardness of the abrasive is about one-half times harder than that of material.

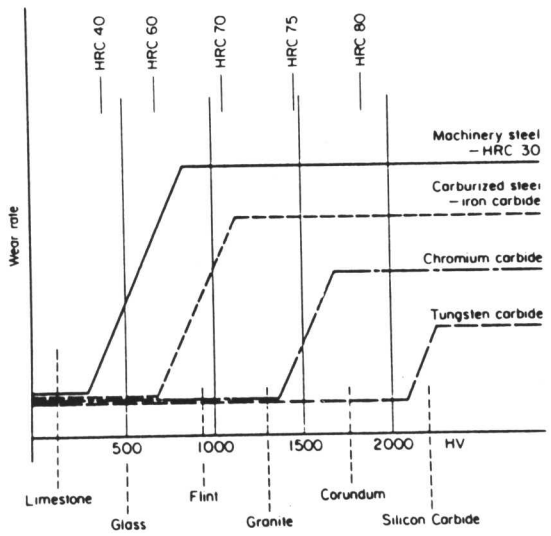

Fig. 6.2: Idealized diagram of wear rate of a variety of materials as a function of mineral abrasive hardness.[9]

Several examples may be given in support of the data presented in Fig. 6.2. For example, Fulcher et al.[10] showed that wear resistance increased with the carbide volume fraction when they used garnet, but decreased when SiC (which was thought to cause spalling and pitting of carbides) was used. Fang et al.[11] studied the abrasive wear resistance of white cast irons using pin-on-disc and wet rubber-wheel-abrasion tests, and suggested that M_7C_3 carbides are particularly effective in resisting wear due to their high hardness. They proposed that the matrix cannot easily be removed in the case of primary carbides, which are firmly held and which resist being cut out by abrasives, resulting in lower volume loss and higher wear resistance. They observed more noticeable increases in wear resistance as a function of the Cr/C ratio (which was thought proportional to hardness) when they used soft abrasive garnet compared with harder abrasive SiC. Therefore, they suggested a critical value of H_c/H_a (hardness ratio of eutectic carbide to abrasive) of 0.8. If the ratio is larger then an effective increase in wear resistance is observed. Kretschmer,[12] Wahl[13] and Su et al.[5] support this proposal, suggesting that a decrease in wear resistance is observed with an increase in the hardness of abrasive. On the other hand, Berns and Fischer[14] have observed a decrease in the wear resistance with increasing bulk hardness of Fe-Cr-

C based alloys after about 850HV, when they used SiC as an abrasive. They explained the decrease in wear resistance by the formation of microcracks around the hard carbides. The same researchers found an increase in wear resistance with increasing hardness when they used flint, which is relatively soft. Similar results were obtained in high Cr cast iron by Xing et al.,[15] who observed effective cutting of M_7C_3 carbides by abrasives when they used SiC and Al_2O_3, but with garnet, only the formation of scratches was observed and there was no indication of carbide breaking and spalling. Kosel et al.[16] demonstrated that carbides tended to protrude at the worn surface when the carbides (≈ 2000 HV) were harder than the quartz abrasive (≈ 1040 HV). Although some protrusion of carbides was observed when they used Al_2O_3 (≈ 2200 HV) this was not as much as with quartz. All these results imply that the contribution of the carbides to the abrasive wear resistance is a function of the hardness of the abrasives. If the abrasives are softer than the carbides then carbides may not be deformed, resulting in relatively good wear resistance. If on the other hand, the abrasives are relatively hard, the carbides may spall giving poor wear resistance. Different test techniques also alter the influence of abrasives. For instance, Sun[17] examined the effect of M_7C_3 carbides on heat treated steel, ordinary white cast iron, and high-chromium cast iron with a wet quartz sand rubber wheel abrasion technique. He observed the formation and expansion of cracks and subsequent spalling of the M_7C_3 carbides, even in a relatively soft quartz abrasive, concluding that some carbides are sufficiently brittle to fracture due to indentation by soft particles. However, he did not take account of the difference expected between dry and wet test conditions. For example, (as suggested by Lin and Qingde[18]) in high Cr alloys (≈ 28 wt%), Cr increases the wet wear resistance more than it increases dry wear resistance implying that corrosion affects the wear characteristics of the alloys. They showed that in corrosive conditions, if the matrix is corroded, its support to the carbides decreases and this may lead to spalling. It is very likely that this mechanism is dominant in Sun's experiments since spalling is unlikely with the relatively soft quartz, which has a hardness (≈ 900 HV) much lower than that of the M_7C_3 (≈ 1800 HV). On the other hand, Fulcher et al.[10] supported Sun's experiments and showed that weight loss begins to increase as soon as the alloy content exceeds the eutectic composition, and that primary M_7C_3 carbides are formed when they used semirounded quartz in the rubber-wheel-abrasion test (RWAT). Their observations showed cracking and spalling of the primary carbides, and they concluded that when this happened the matrix was worn to a higher degree. Although large carbides resisted better than the matrix, this only continued until the cracks started to form. Since carbides protruded at the wear surface, with the reduced support from matrix, they were more vulnerable to cracking, and this phenomenon was thought primarily responsible for low wear resistance in hypereutectic cast irons when using semirounded quartz abrasives.[10] The opposite results were observed by Prasad and Kosel,[19] who suggested that protruding carbides protect the matrix from direct contact with the quartz abrasives, and since the carbides concerned have a higher hardness than quartz, no noticeable damage was observed. These experiments clearly indicated the material removal mechanisms in hypereutectic

white cast irons containing primary M_7C_3 carbides when they performed in situ scratch testing using rounded quartz particles as scratch tools in a scanning electron microscope. During multiple scratch testing of preworn hypereutectic alloys containing pits and cracks (which probably formed in pre RWAT abrasion), cracks were found to develop near the entrance region of the pre-existing pits, with no sign of carbide removal. As the multiple scratches progressed along the same path, small carbide fragments began to appear near the pre-existing pits, implying the gradual enlargement of pits rather than catastrophic damage of primary carbides. Prasad and Kosel[19] also tested the same alloys in the absence of pre-existing pits, and groove cracking, and showed an increase in the amount of debris particles with the passes. These debris particles were found to contain a significant amount of Si, implying that they are mainly quartz fragments. Indeed energy dispersive X-ray analysis showed that there was no sign of carbide debris in the particles. Additionally, they observed no pit formation on the carbide beneath the quartz particles. These results indicate that rounded quartz particles are not capable of causing spalling in the primary carbides, contrary to Sun[17] and Fulcher's et al.[10] observations. Prasad and Kosel suggested that the matrix was not directly attacked by the abrasives until some carbide removal had occurred, following which, cracks were observed at the carbide/matrix interface due to reduced support from the matrix. They deliberately deep etched the alloys (hence removing the matrix) and it was then possible to observe the material removal mechanism for unsupported carbides. Their results showed the formation of cracks at the leading edges of the primary carbides. Although Fulcher et al.[10] agree with this observation (that less supported carbides are more vulnerable to cracking), initial cracking and spalling off the carbides in their experiments are not consistent with Prasad and Kosel's direct, in situ experimental results. Carbide removal under the quartz particles may be attributed to a difference in the abrasive shapes. Prasad and Kosel suggested that some rounded quartz particles can be fractured, and these may initiate carbide fracture due to their greater angularity. This proposal is quite likely to be correct and in fact Moore et al.[20] showed between 2 and 5.5 times greater wear rate with the angular crashed quartz than rounded Ottawa sand, probably due to the deteriorating behaviour of angular abrasives and because of high contact distance. A similar conclusion was reached by Swanson and Klann,[21] who showed an increase by a factor of ten in the volume loss when they used angular abrasives on plain carbon and low alloy steels. Since both plastic deformation and fracture mechanisms cause material removal of brittle solids during wear, and material loss is an order of magnitude greater when fracture mechanisms are dominant,[22] poor wear resistance could be explained by the sharp abrasives, which lead to carbide cracking and subsequent spalling. Although these results may explain the difference between the work of Sun,[17] Fulcher et al.[10] and that of Prasad and Kosel,[19] (since the former investigators used sub-angular quartz abrasives, but in the latter's work a rounded quartz abrasive was used), more work definitely needed to verify whether angular quartz abrasives cause formation of cracks and spalling off the primary M_7C_3 carbides in hypereutectic iron-based hardfacing alloys.

As far as the hardness of the carbides is concerned, it is feasible to suggest that maximum hardness should be considered to be the hardness of the undeformed carbides, as Richardson[23] has proposed.

6.2.2 Effect of Carbide Size

It has been suggested that carbide hardness is an insufficient indication of wear resistance, because a decrease in hardness is accompanied by a rise in particle size, at constant volume.[24] However, the material removal mechanisms for fine and coarse carbides have been found to be associated with the increasing ratio between average groove depth and carbide size as carbide size decreases.[25-27] Shetty et al.[25] examined the material removal mechanisms during the abrasion of Stellite 6 and 19, with a scratch test using Al_2O_3 abrasive particles and Vickers diamond pyramids. In the case of fine carbides, they observed the removal of entire small carbides within primary chips, but for coarse carbides, abrasive particles had to cut the carbide phase to remove either the carbide or matrix phases, since the scratch groove dimensions are then smaller than the carbides. In these circumstances, coarser carbides cause an increase in wear resistance. Desai et al.[26] studied the same alloys containing coarse carbides, using a low-stress abrasion test with Al_2O_3, and found the carbides to protrude from the worn surface. However, for fine carbide specimens, carbides were abraded to the same level as the matrix, and there was no marked indication of changes in the widths of wear grooves as they traversed the matrix and carbides. This results in more frequent pit formation and poor wear resistance. Shetty et al.[25] suggested that the linkage of cracks along the carbide/matrix interface may play a secondary role in material removal from fine carbide containing alloys. They showed crack propagation from carbide to carbide and along the carbide/matrix interface resulting in the formation of pits which contain several small carbides. They proposed that a strong carbide/matrix interface is also necessary for enhanced wear resistance. Zum Gahr and Doane[28] agree with their proposal, claiming that early crack formation at the carbide/matrix interface may decrease wear resistance. Junyi and Yuding[27] examined the effect of carbide size on wear resistance in undirectionally solidified high Cr (16.2Cr and 3.35C wt%) cast irons. They measured the average spacing between carbides, representing average carbide thickness at constant carbide volume fraction. Consistent with Shetty et al.,[25] and Desai et al.[26] they showed that fine carbides are not resistant to abrasives, and wear resistance decreases due to bending and deformation. On the other hand, they observed spalling of thick carbides, resulting in less protection being given by the carbides to the matrices, when they used the rubber-wheel-test with wet sand. Therefore, they suggested that carbide fibers should be of an optimum size, below which they are not deformed and above which they must resist spalling.

Sun[17] showed an increase in weight loss in the presence of coarse carbides due to spalling when they applied the wet sand rubber-wheel-test in high Cr white cast irons, consistent with Junyi and Yuding.[27] It should be noted, however, that both Junyi et al., and Sun's experiments were carried out in wet sand. As discussed previously, the corrosive behaviour of the matrix can

be important and may effect these results. Coarser carbides obviously have a more continuous carbide/matrix interface. If the support from matrix is decreased due to corrosion of the matrix this may lead to subsequent spalling. Garrett et al.[29] using the pin-on-disc technique, showed a decrease in relative abrasion resistance as the total carbon concentration increased. They suggested that the higher carbon concentration gave coarser carbides, resulting in a lower wear resistance, but this is inconsistent with the work,[24-26] where better wear resistance was obtained with larger carbides. One difficulty is that Garrett et al's[29] alloys covered a wide range of microstructures (dendritic, eutectic, and primary carbides) which behave in different ways under the same test conditions. Without taking into account microstructural factors, it is not feasible to represent the abrasive wear resistance as a function of total alloy carbon concentration. Even so, the beneficial effect of increasing carbon content of a wide range of ferrous materials has been demonstrated (Fig. 6.3).

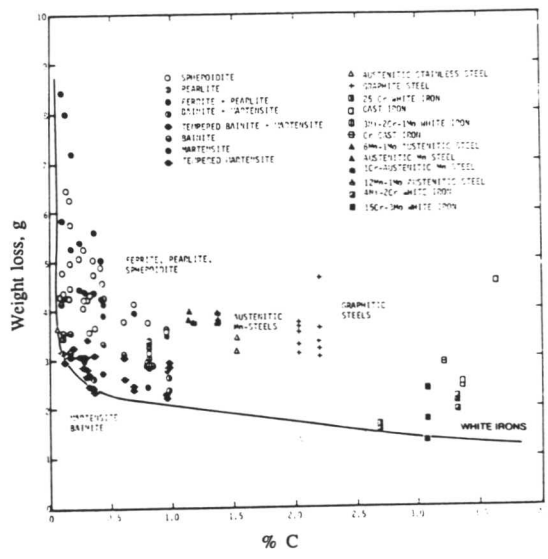

Fig. 6.3: Weight loss versus carbon content of a wide range of ferrous materials after a wet sand slurry abrasion test.[4]

6.2.3 Effect of Cooling Rate

Since wear resistance is strongly affected by the carbide size, the cooling rate apparently has a significant influence. Gundlach and Parks[30] examined the effect of the cooling rate on abrasive wear resistance in white cast irons (Fe-17.5Cr-1.5Mo-2.9C wt%) and observed an initial increase in wear resistance with decreasing cooling rate, and subsequently a decrease. They suggested that the cooling rate influences the carbon concentration of the austenite, and results to secondary carbide formation upon slow cooling. On the other hand, a higher dissolved carbon content and a higher volume fraction of retained austenite were observed with fast cooling rates. However, they could not verify a relationship between the microstructure and abrasive wear resistance under different cooling rates. As already discussed, the best explanation could be made by considering the effect of the cooling rate on the carbide size. They may have observed the initial increase in wear resistance with decreasing cooling rate because of the increase in carbide size which gives higher resistance to cutting out by abrasives. Spalling of the carbides may be responsible for the later decrease in wear resistance, but it is difficult to say without careful microstructural observations.

The effect of the cooling rate on the abrasive wear resistance was studied by Kortelev et al.,[31] Popov et al.,[32] and Drzeniek et al.[33] in high Cr iron-based hardfacing alloys. However, explanation of the test results is a matter of conflict. For example, Kortelev et al.[31] examined microstructural changes of Fe-(40-42)Cr-(4.0-4.3)C (wt%) hardfacing alloys under different cooling rates. They found significant refinement of carbides with increasing cooling rate from 10 to 28.9 ^{o}C/sec, and a corresponding 30-35% increase in the abrasive wear resistance. Their quantitative metallographic analysis showed that at 10 ^{o}C/sec cooling rate, 60% of the carbide area was found to exceed 2500μm^2, whereas with a high cooling rate (28.9 ^{o}C/sec), the majority of the carbides had an area between 250-1500μm^2. They carried out the abrasive wear tests simulating the working conditions for rotary excavator cutters. Their test results showed a continuous increase of the abrasive wear resistance with increasing cooling rate. They suggested that grain refinement, and differences in the carbide lattice structure were probably the dominant factors responsible for the improved wear resistance. Although the carbide refinement was experimentally observed, there was no evidence for the changes in the carbide lattice structure. Since they have not examined the worn surfaces, it is not feasible to directly correlate the abrasive wear resistance with the carbide area in their work. On the other hand, an increase in the abrasive wear resistance with cooling rate was explained on the basis of changes of matrix structure by Drzeniek et al.[33] They studied the influence of the cooling rate in high Cr containing iron-based alloy (Fe-22.05Cr-4.44C-1.61Mn-0.35Si wt%), with arc welding technique using self shielded cored electrodes. The cooling rate was altered by adjusting the preheat temperature of the substrate. With high cooling rates the austenite transformed to martensite. Whereas at lower cooling rates the austenitic matrix decomposed into pearlite. Using the rubber-wheel-abrasion test with quartz sharp edged sand, the weight loss was found to be about 3 times higher with the slow

cooling rate. They suggested that pearlite formation is a major factor decreasing the wear resistance although they did not analyse any changes in carbide particle size. As discussed earlier, fast cooling rates lead to the formation of relatively finer microstructures. Although the abrasive wear resistance of the austenitic matrix was reported to be superior than that of the pearlite, influence of carbide size has to be considered for interpretation of the experimental results.

As far as the effect of carbide size on wear resistance is concerned, fine carbides tend to be cut out by hard abrasives so that abrasive wear resistance increases with carbide size, particularly in high Cr alloys having a large volume fraction of M_7C_3 carbides. Nevertheless, much coarser carbides may be spalled off under certain abrasive wear conditions, implying that an optimum size of carbides is desirable for best wear resistance. Since the size of the carbides has an important effect on wear resistance, the surfacing process and its parameters should also be chosen carefully in order to obtain the best abrasion resistance.

6.2.4 Effect of Carbide Spacing

Besides the effects of hardness and shape of the carbides, carbide spacing has an important effect on abrasive wear resistance as well. Although Bhansali and Silence[34] suggested that abrasive wear resistance increases when the average spacing between precipitates is increased, this is contrary to experimental observations.[10,35,36] For instance, Fig. 6.4 illustrates the dependence of wear resistance and hardness on the mean free path between carbides in different annealed tool steels.[35] As can be seen in Fig. 6.4 wear resistance increases as the mean free path between the carbides decreases.

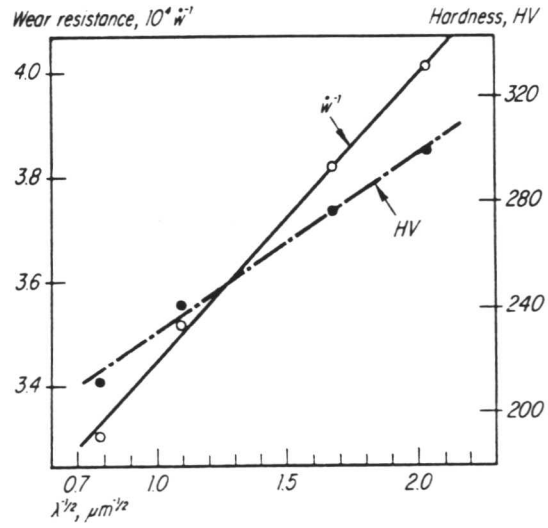

Fig. 6.4: Dependence of wear resistance and hardness on the mean free path between carbides in tool steel.[35]

Fulcher et al.[10] suggested that finely spaced eutectic carbides in hypoeutectic high Cr-Mo white cast irons support the matrix and prevent penetration by the abrasive particles, and it has also been suggested that the deformation of the matrix is decreased as the carbide spacing decreases in white cast irons.[36] Mello et al.[36] emphasized the importance of carbide spacing in abrasive wear resistance of Cr-Mo white cast irons when they carried out sclerometric experiments.[1] They estimated scratch hardness values of carbide and matrix phases from the force data, (obtained by using a three-dimensional piezoelectric sensor) and the mean groove width values.[2] They examined different areas with various carbide spacings, λ, in the range 2 to 127μm, and measured the corresponding groove width in the matrix. The variation of scratch hardness was represented as a function of the ratio L/λ, at two different loads (1.0N and 0.25N), and at a constant scratch speed ($125\mu ms^{-1}$), in a high Cr iron-based alloy (Fe-21.4Cr-2.36C-2.98Mo-1.04Mn-0.54Si wt%) having primary γ dendrites, and 0.24 volume fraction of M_7C_3 eutectic carbides. Their results showed three main regions: in the first region, the scratch hardness values corresponding to the wider carbide spacing were found to be nearly constant, and close to that of the matrix, implying no contribution of carbide to hardness. After a critical value of L/λ, the scratch hardness started to increase with a decrease in carbide spacing, forming the second region, and finally the hardness reached its maximum value, corresponding to the smallest carbide spacing, and remained constant at a value close to the scratch hardness of the carbides. These results quite clearly indicate that closely spaced carbides significantly support the matrix, and reduce its ability to undergo plastic flow.

6.2.5 Effect of Carbide Volume Fraction

The influence of carbide volume fraction on abrasive wear resistance is controversial. This has been studied by many researchers both in welding consumables and in cast structures. Rense et al.[37] suggested that the volume fraction of primary carbides is of fundamental importance to combatting abrasive wear. They showed that weight loss decreases until 0.5 carbide volume fraction, but Zum Gahr and Doane[28] observed a decrease in volume loss after 0.3 carbide volume fraction in austenitic as well as martensitic white irons in the rubber-wheel test. Noble[38] suggested that the difference between the weld deposits and white cast irons may arise due to different cooling rates, which leads to different carbide sizes and morphologies. Zum Gahr[39] showed that abrasive wear resistance increased with increasing volume fraction of carbides against garnet in white cast irons. Similar results were observed by Xing et al.[40] who showed that when alloys are tested against very hard abrasives, such as SiC and Al_2O_3, an increase in carbide volume fraction increases wear resistance slightly. However, when tested against garnet (whose

---

1 Sclerometric experiments are single-point scratch test which simulates abrasive-target interactions.

2 The scratch hardness (H_s) was given by the following expression;

$$H_s = 0.7F_nL^{-2} \qquad .....(1)$$

where, F_n is the normal force and L is the mean groove width.

hardness is much lower than that of M_7C_3 carbides) an increase in the volume fraction of carbides cause a pronounced increase in wear resistance. Borik and Majetich[41] studied the effect of volume fraction of carbides, and of bulk hardness, on weight loss in rubber-wheel-abrasion tests and pin-on tests on iron-based hardfacing alloys. They observed that in the rubber-wheel tests weight loss decreased with an increase of carbide volume fraction to 0.45 and later increased, whereas the transition volume fraction was found to be 0.55 for the pin-tests. Similar results were found by Zum Gahr and Eldis,[42] who showed the lowest wear loss with a carbide volume fraction of 0.30 in the rubber-wheel-abrasion test, but in the pin abrasion test (using 150 mesh garnet) increasing carbide volume fraction up to $\approx$ 50% gave rise to higher wear resistance. He suggested that grooving was dominant in the pin-test, but grooving and spalling both occurred in the rubber-wheel test. This could be explained by the effect of wet sands which were used in both the works of Borik et al.,[41] and Zum Gahr et al.[42] These results quite clearly indicate that the effect of volume fraction of carbides depends upon the applied wear test conditions. If the applied abrasives are hard enough to deform the carbides, an increase in volume fraction may lead to a great chance of formation of cracks or spalling, and subsequently a lower wear resistance. Fig. 6.5 shows the effect of volume fraction of carbides on volume loss of high chromium-molybdenum white irons. It is illustrated that if the hardness of the abrasive (garnet) is less than that of the carbides the wear resistance increases with carbide volume fraction in both austenitic and martensitic matrix. However, the opposite is the case when SiC abrasives are applied. This occurs due to high hardness of the SiC abrasives which cause spalling off carbides and results in more vulnerable matrix to fracture.

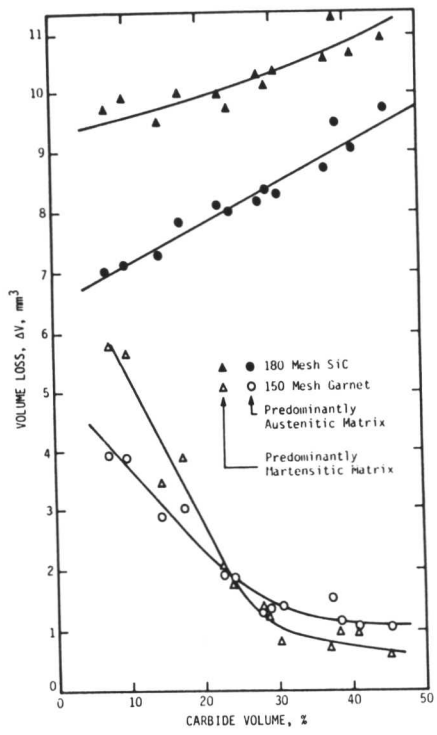

Fig. 6.5: Effect of carbide volume fraction in the volume loss of high chromium- molybdenum white irons due to abrasion with 150 mesh garnet and 180 mesh SiC abrasives.[4]

However, Fulcher et al.[10] found an increase in wear resistance in hypoeutectic alloys when they used the both abrasives, proposing that eutectic carbides support the matrix, and any increase in volume fraction of carbides provides better support and wear resistance. Noble[43] examined the effect of microstructure on abrasive wear resistance in steel and high Cr austenitic alloys which were deposited by the flux-cored arc welding technique. With the high Cr alloys he carried out wear test experiments in wet and dry coke abrasives and showed a decrease in relative wear life with increasing volume fraction of primary Cr carbides. He suggested that the carbides were worn at the same rate as the matrix, and also the carbides may be brittle, and they cannot accommodate plastic strain giving rise to a high weight loss. Finally, he suggested on the grounds of his experimental results that it may be necessary to reduce the overall alloy content in order to obtain less volume fraction of primary Cr carbides in the weld deposits. On the other hand, it would seem that, there are some discrepancies in his experiments. First of all, with high Cr austenitic irons, there is a high amount of NbC (from 6% to 12%), which strongly influences wear resistance and this will be discussed later on. Without taking into account the effect of NbC on wear resistance, it is not feasible to derive his final conclusion. Secondly, the alloys which were

marked as a W116 (Fe-23.3Cr-5.1C-5.5Nb-1.04Si wt% and others) and W117 (Fe-23.4Cr-5.1C-6.2Nb-1.1Si wt% and others) have quite similar compositions and the same volume fraction of primary Cr carbides (43%). However, average wear life of the alloy W117 is ≈ 58% higher than alloy W116 when tested in the dry coke. When we consider the effect of NbC volume fraction we can not find any correlation, because the NbC volume fraction is only 1.5% higher in alloy W117. On the other hand, there is no significant difference in microhardness of the carbide and matrix phases either. In addition to this, the relative wear life of W117 is much higher than alloy W115, even though the Cr carbide volume fraction is significantly greater in the alloy W115. This implies a discrepancy between his conclusion and the dry coke wear test results. A similar example may be given for alloys W121 and W123, both having 37% Cr carbide and 9% NbC volume fractions, where the wear life of the alloy W121 is 33% higher than alloy W123 in wet coke experiments. If this error came from his experimental technique, his results are not good enough to represent the dependence of volume fraction of Cr carbides on wear life; at least not as good as to conclude that wear resistance decreases as the volume fraction of Cr carbides increases. Perhaps the best explanation could be made by taking into account the important role of matrix in giving support (the best wear resistance being obtained in the case of strongest support from the matrix as he suggested). Although Garrett et al.[29] made a similar suggestion by concluding that the increase in the concentration of % total carbide forming elements does not increase wear resistance in a wide range of iron-based alloys (hypoeutectic, eutectic, and alloys with primary carbides), their results do not rely upon any microstructural observation. On the other hand, they concluded that highly alloyed irons (which they refer to as expensive alloys) are not necessary for good wear resistance. This conclusion seems to be quite unscientific and ignores the importance of other issues such as the different abrasive wear behaviour of the same alloys in different tests, changes in the wear mechanisms with test variety and other desirable properties (e.g. oxidation and corrosion resistance, matrix stability) of the hardfaced alloys.

Before discussing the effect of other parameters on wear resistance, it is possible to conclude briefly that the volume fraction of the carbides is one of the important criteria influencing wear resistance in one way or another, but should be considered in conjunction with the other variables.

6.2.6 Effect of Carbide Anisotropy

Wear behaviour of crystalline hard materials is generally anisotropic. For example, in SiC and TiO_2, experimental results have shown that wear depends on crystallographic orientation, since wear resistance is higher on the planes of highest atomic density when sliding occurs in the most closely packed direction.[44] As well as the crystalline anisotropy, structural anisotropy can occur, and is generally observed in aligned fiber composites as a result of undirectional solidification. For instance, in samples where the carbide fibers were undirectionally arranged, Junyi and Yuding[27] found better wear resistance, when the exposed surface was perpendicular to the carbide fibers. This is because these fibers are firmly supported, not easily broken and not susceptible to

spalling. Su et al.[5] support this proposal in their work on undirectionally solidified high Cr irons. They found better wear resistance when the wearing surface was perpendicular to the carbide fibers. It has also been reported that[45] the orientation of the [001] axis of the carbides, in a direction normal to the wear plane gives a higher wear resistance than when the same axis lies in the plane of wear and parallel to the wear direction.

6.3 Effect of Matrix Structure

Since the carbides are discontinuous in the structure a main role of the matrix is to support carbides. For iron-based alloys the abrasive wear resistance increases progressively as the matrix changes from ferrite to pearlite, bainite, and martensite.[46] Ferrite has a lower wear resistance due to its low hardness. Gundlach and Parks[30] showed that martensitic irons have better wear resistance than austenitic irons. Diesburg and Borik,[47] and Dawson et al.[48] suggested that martensite is the preferred structure for improving abrasion resistance in steels. The highest wear resistance was found with a martensitic matrix, or a tempered martensitic matrix due to high hardness values. However, at equal hardness, bainitic microstructures which isothermally transformed to lower bainite were found to have a much better wear resistance than martensitic microstructures. Zum Gahr[46] contributed this behaviour to the presence of 20% retained austenite in the bainitic structure. In fact other investigators have also observed enhancement in wear resistance with an increase in volume fraction of retained austenite in steels.[49-51] The following general conclusions have been made in order to explain the beneficial effect of retained austenite:

- transformation induced plasticity may absorb energy which might otherwise have caused fracture. The transformation may also induce compressive stresses in the surface and hence retards microcrack formation;
- the increase in the work hardening rate with strain as a result of the austenite-martensite transformation increases wear resistance;
- the presence of ductile austenite films around the martensite plates impedes microcrack formation and growth.

Bhadeshia and Edmonds[52] suggested that those alloys which have a mixture of bainitic ferrite and stable carbon-enriched austenite give improved strength and toughness properties over those of conventional tempered martensite microstructures, since in these alloys the cracks have to traverse not only finely spaced interphase interfaces, but also different crystal structures. Consistent with this, Salesky and Thomas[53] showed better abrasive wear resistance with an increased retained austenite content in martensitic steels. They proposed the existence of a relationship between the continuous interlath films of retained austenite with increasing wear resistance. However, the complexity of the relation between abrasive wear resistance and retained austenite is present in other experimental results.[30,54,55] For example, Zum-Gahr[54] studied the effect of retained austenite (retained γ) on the abrasive wear resistance of a Fe-Mn-Cr-V tool steel, using pin-like samples abraded against 70μm Al_2O_3 bounded abrasive discs, simulating

high-stress or grinding abrasion test.[56] The best abrasion resistance was found at an intermediate retained austenite content (between 16 to 26%), attributed to the formation of martensite during wear, causing compressive stresses which retard the formation of microcracks. On the other hand, Gundlach and Parks[30] found that an alloy with a bainitic-like matrix had the poorest wear resistance against SiC, Al_2O_3, and Garnet abrasives using the high stress AMAX pin test (APT).[3] However, against SiC, and Al_2O_3, irons with retained austenite were found to be superior to martensitic irons, but against the softer garnet abrasive, the martensitic irons had a better wear resistance.

Besides the effect of different abrasives, the influence of various types of abrasive wear was emphasized by Fiore et al.,[55] who studied low-stress abrasion, and gouging wear of Ni-Cr white iron, which contained angular M_7C_3 carbides and retained γ in the range of 5 to 85 vol%, together with other decomposition products of austenite.[4] Their low-stress RWAT abrasion tests with SiO_2, Al_2O_3, and the gouging test results are given in Fig. 6.6, which includes high stress AMAX pin test (APT) on Al_2O_3, and garnet papers.

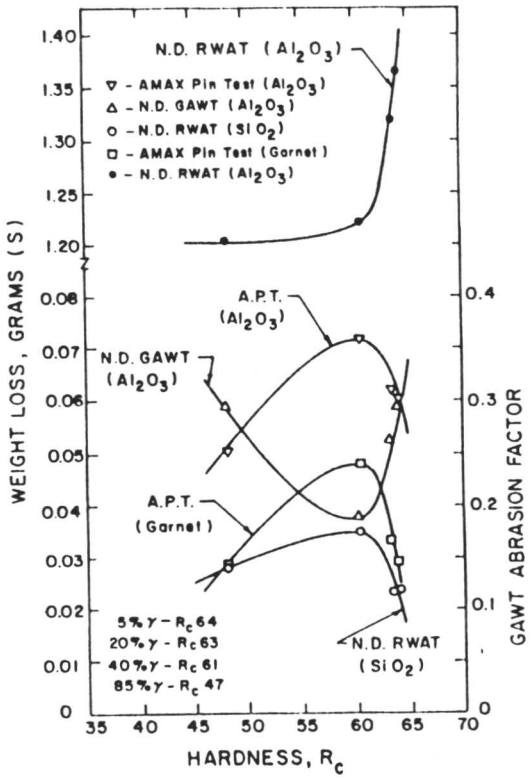

Fig. 6.6: RWAT, APT and GAWT abrasive wear test results of Ni-Hard samples (Fe-8.9Cr-5.86Ni-3.22C-1.77Si-0.55Mn wt%).[56]

[3] In this test, a pin-like sample traverses back and forth against a bonded abrasive paper, simulating grinding wear.

[4] In gouging wear test experiments, abrasives are rigidly supported as they plough through the material which is generally subjected to high impact conditions.

As is seen in Fig. 6.6, the percentage of retained austenite decreases towards the right on hardness axis. The minimum in weight loss occurs at 40% retained γ with the RWAT test against SiO_2. However, the worn surface examinations at four different retained austenite levels revealed identical surface topographies. Observations showed a deep groove formation in the matrix, with the carbides protruding and probably being worn gradually rather than by gross fracture. On the other hand, with the harder Al_2O_3 as the abrasive the weight loss increased with hardness (associated with the decrease in volume fraction of retained austenite); the harder alumina was shown to be effective in cutting the matrix and carbide phases. They found almost identical worn surface characteristics at different retained austenite levels. A similar conclusion was reached with GAWT tests, in spite of the significant differences in weight losses. The chipping of material from the leading edges of protruding carbides was considered to be the important parameter in the RWAT SiO_2 test, since the matrix is abraded and cannot adequately support the carbides. With Al_2O_3, there was no indication of carbide relief and both phases were almost worn at the same rate. During the GAWT test, material is removed by a micromachining action. They also suggested that the rake angle of the abrasive particles, the critical rake angles of the various microconstituents, thermal effects on the microstructure, and stress-induced transformation of retained austenite to martensite are important variables. Even though they concluded that retained austenite content may optimise wear resistance in different abrasive situations, their explanations on the basis of the effect of retained austenite is not convincing. For instance, to assume the variation of total hardness only as a function of volume fraction of retained austenite means ignorance of the contribution of other phases. This is because, it is reasonable to accept that total hardness is a linear combination of the contribution from the individual components. It is probable that the influence of the retained austenite is associated with other phases present in a microstructure, and best understood by a careful examination of initial microstructure as well as wear test conditions. As it has been shown by Bhadeshia and Edmonds[52] even different retained austenite morphologies significantly influence impact properties of the bainitic steels. They studied the alloys containing only bainitic ferrite, retained austenite, and some martensite as confirmed by transmission electron microscopy. In such a microstructure, retained austenite was found either in a blocky morphology bounded by crystallographic variants of bainitic sheaves or in films of austenite between the subunits within a given sheaf of bainite. When the specimens were stressed at various levels without fracture or necking, the thin films of austenite between the bainitic ferrite subunits remained untransformed, but the irregular blocky austenite decomposed to untempered martensite as a result of stress-induced transformation of the prior retained austenite. This clearly indicates that the film austenite is more stable than the corresponding blocky morphology, and beneficial as far as the toughness is concerned. Bhadeshia and Edmonds[52] finally summarised the criterion for optimum properties by the following equation;

$$(V_{\gamma\ -f} / V_{\gamma\ -B}) = V_B / ((6\text{-}7.7V_B) > 0.9 \qquad .....(2)$$

where

$V_{\gamma\ -f}$: volume fraction of the film type retained austenite,

$V_{\gamma\ -B}$: volume fraction of the blocky type retained austenite,

V_B : volume fraction of bainitic ferrite.

This equation indicates that the best properties for toughness is expected when the ratio of $((V_{\gamma\ -f} / V_{\gamma\ -B})$ is a maximum. Considering the same phenomenon in wear resistance, blocky morphology may be desirable. This is because, it is unstable under stress, and transforms to stress-induced martensite, which generally increases low-stress abrasion, and grinding wear resistance. On the other hand, under the gouging wear conditions blocky morphology may be detrimental, since in these test conditions material is subjected to impact conditions. However, optimum conditions have to be carefully examined for better wear resistance. In white cast irons, the best abrasive wear resistance was obtained with the martensitic matrix, and the worst with an austenitic matrix by Zum Gahr and Doane.[28] They suggested an optimum matrix as being hard but not too brittle in order to prevent early cracking of the massive carbides, or at the carbide/matrix interface during deformation.

6.3.1 The Role of the Carbide/Matrix Interface

It has been shown[57] that there are three main considerations with respect to crack propagation; the nature of the matrix, the carbide/matrix interface, and cleavage planes of massive carbides. Fig. 6.7, shows schematically the strain energy release rate (crack growth rate) of white cast irons, and of the proportion of the matrix, the interfaces, and the carbides as a function of primary carbide volume fraction.

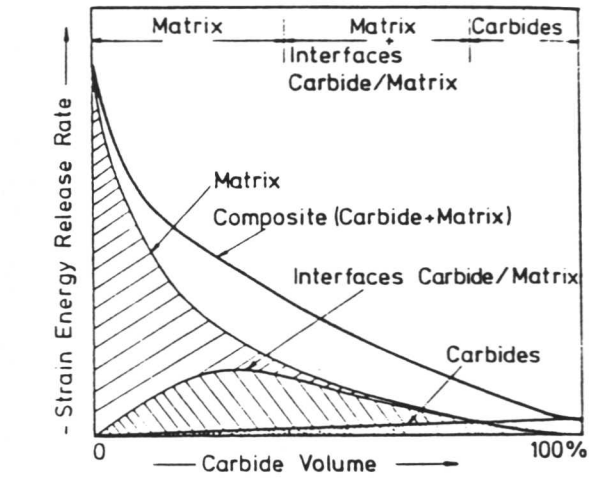

Fig. 6.7: Schematic representation of strain energy release rate of white cast irons and of the proportions of the matrices and the carbides as a function of % primary carbide volume.[57]

At small carbide volume fractions matrix, but at medium volume fractions matrix and interfaces are dominant phases at which the strain energy is released fast. The contribution of the carbides is only significant at higher volume fractions. Since hypereutectic Fe-based hardfacing alloys contain a volume fraction of primary carbides at a medium level, it is clear that carbide/matrix interface has a considerable influence on the strain energy release rate and crack propagation. Therefore strong interfaces (low carbide/matrix interfacial energy[46]) are needed for better wear resistance.

Although the importance of the carbide/matrix interface on wear resistance is often emphasized methods for controlling interface properties are not clear. In many cases, especially under heavy abrasive conditions, cracks initiate at the interfaces due to high stress concentrations in these regions. In addition to the high stress regions at the sharp interface edges, differences in the thermal expansion coefficients of the carbide and matrix phases cause a buildup of substantial residual stresses,[58] which may reach a level high enough to break the interfacial bonds.[59] For example, the thermal expansion coefficient of M_7C_3 carbide is much lower than that of the ferrite and austenite phases (e.g. for ferrite 12.3 10^{-6} K^{-1}, and for M_7C_3 8.8 10^{-6} K^{-1} at 100^oC[60]) implying that the stresses arise at the interfaces. During wear, if the stresses increase in

the interface debonding may occurs between the matrix and carbide phases. This leads to crack formation along the debonded surface, and subsequently the cracks may propagate across the whole carbide, resulting in a higher weight loss. In order to lower the residual stresses, the quenched-and-tempered materials were thought to be beneficial, since volume expansion associated with the transformation (e.g. martensitic transformation) tends to lessen the influence of differences in the thermal expansion coefficients of phases.[58]

Besides the effect of a difference in thermal expansion coefficients of carbide and matrix phases, there is a strong influence of chemical segregation, which if it occurs at the interfaces, it can reduce the surface energy and lower cohesive strength, or fracture stress of the interfaces.[61] It is well known that cracks can propagate much easily in a cohesively weak interface, as confirmed by experimental observations, which showed formation of interfacial cracks at the particle-matrix interfaces at lower stresses and strains due to low cohesive strengths.[62-64] As far as the Cr carbides are concerned, experimental studies show a strong tendency of segregation of solute atoms at matrix/carbide interface (e.g P, C, Cr segregation to γ /M_7C_3 interface[65], Si segregation to γ /M_7C_3 [66] and Cr carbide/matrix interface[67]). Since it is well established that segregation at the interfaces decrease cohesive strength and cause weak bonding and easy fracture,[61,68] segregation should be kept at a minimum level, to avoid early cracking in carbide-matrix interface. Unlike hardfacing alloys, interfacial phenomenon has taken great interest in metal-matrix composites. In these alloys it is believed that the matrix with a higher yield strength tends to reduce the interface crack displacement, leading to the low stress concentration factor at the fiber end of the interface crack.[58] This reminds us of the effect of martensite on abrasive wear resistance. Experimental results showed that martensitic matrix was superior to other matrices (e.g. pearlite, ferrite) and this was thought to be a result of the high hardness of martensite. On the other hand, its high yield strength may play an important role on the abrasive wear resistance similar to metal-matrix composites.

There is no doubt that good support from matrix for the more brittle carbides is necessary. Fulcher et al.[10] in high Cr-Mo cast irons, Noble[43] in low alloy steels and in high Cr austenitic iron deposits, Rakayby and Mills[69] in high speed steels, and Lin and Qingde[18] in high Cr cast irons suggested that abrasive wear resistance is increased as long as eutectic or primary carbides are well supported by the matrix to prevent cracking and subsequent material removal. Rakayby and Mills[69] showed that when the matrix was in its strongest state it could not be ploughed by the abrasives, and so, the matrix was able to hold carbides and prevent material loss.

On the other hand Lin and Qingde's[19] results are in conflict as far as the effect of matrix structure on abrasive wear resistance is concerned. They examined the corrosion-abrasion resistance of cast iron containing up to 2%Cu, and the effect of austenitic, martensitic, and as-cast matrices on abrasive wear resistance by using the pin-disk abrasion test with SiC and garnet. They found higher wear resistance in the alloys having the austenitic matrix than martensitic alloys when the hard abrasive (SiC) was used, but not when a softer abrasive (garnet) was used.

When the abrasive was soft, an increase in volume fraction of carbides led to increased wear resistance particularly when the matrix was austenitic. In the case of hard abrasives, the wear mechanism corresponded to microploughing with its associated high rate of weight loss. When soft abrasives were used, the carbides protruded during wear which was controlled by the matrix. Although support from the austenite was inferior to martensite, it was shown that support from austenite is increased by work hardening during wear, the work hardened layer having a depth of 50μm. It should be noted that although the work hardened layer is beneficial in many cases, the depth of the hardened layer is shallower than required for service applications[70] (3-5mm in austenitic balls in grinding mills). Shepperson and Allen[71] proposed that high strain can be accommodated with the stress induced transformation of austenite to martensite giving better wear resistance in austempered spheroidal cast irons. Lenel and Knott[72] showed good relative wear resistance of the austenitic steels because of their work hardening characteristics. They studied the steels which have a composition around 12Cr-10Mn-0.2N wt%, and found strong work hardening as a result of transformation from unstable austenite to nitrogen-strengthened martensite and therefore superior wear resistance.

These results clearly indicate that if the austenitic matrix has a work hardenable character, it could be preferred to a martensitic matrix as long as sufficient work hardening depth is achieved.

6.3.2 Effect of Matrix Anisotropy

Abrasive wear resistance can be minimized by adjusting the plane and direction of sliding with respect to the microstructure.[73] It has been reported that with an oriented structure, the long term strength at high temperatures can increase by 50%, and the impact toughness by a factor of 2-3 can be improved in the cast gas turbine vanes.[74] Also, the total service life of these vanes increased by 3-5 times that of a non oriented cast structure. However, there are only a few experimental works concerning the influence of matrix anisotropy on wear resistance. Schmidt and Hinsberger[75] examined the isotropic and anisotropic ferrite-martensite microstructures in a Fe-8Ni-0.37C wt% alloys for abrasive wear resistance. Anisotropy was characterised by the orientation dependence of the mean intercept length of the martensitic regions. The anisotropic microstructure was found to be better than the isotropic one and they observed significant direction and orientation dependent differences in the wear resistance. They found no correlation between the wear resistance and the corresponding intercepth length of both phases in order to explain the directionality of the wear rate, and neither with hardness. They proposed that the microstructure and its orientation dependence plays a major role in wear resistance. The wear resistance was found to be a function of the orientation of the long axes of martensite plates with respect to the sliding direction. The highest wear resistance arose when the long axe of martensite plates was oriented normal to the sliding direction since this leads to higher energy dissipation. Vasil'ev[74] studied the dependence of the wear resistance of the columnar structure on the position of the crystal, related to the wearing surface, as determined by the contact angle, α, between the axis of the columnar crystal and the normal to the wear surface. Test results showed that highest

wear resistance is obtained when wear takes place against the direction of the columnar crystals (α=0), whereas, when the direction of wear is perpendicular to the axis of the columnar crystal (α=90^{o}), minimum wear resistance is observed.

Although anisotropy has a great influence on abrasive wear resistance, it is quite difficult to design complex microstructures in practice.

6.3.3 Effect of Subsurface Deformation Characteristics

When we consider the effect of matrix on wear resistance, its subsurface deformation properties have to be understood since the effect is created by abrasives well below the surface. Parameters such as strain, strain-rate, stress, and temperature vary with depth, and significantly influence surface deformation characteristics.[56] For example, the strength of the matrix is reduced by an increase in temperature, resulting in more ductile behaviour. Obviously a high plastic strain rate ahead of an abrasive will cause a localised increase in temperature, and softening. Therefore, further deformation is concentrated in this zone and material shears by forming the shear bands. Subsequently, shear is activated on a new plane, starting from the edge of the abrasive tip, and as this deformation mechanism continues, characteristic lamellar structures are finally observed.[56] This is believed to be due to periodic shear localisation as a result of thermal instability. In the case of high strain rates, there is not enough time for appreciable heat flow to occur and this may lead to adiabatic shear conditions.[76] Soderberg et al.[77] observed segmented chip formation only in the precipitation-strengthened material in 6061 Al alloy, along well-defined shear zones with high strain densities. They suggested that in spite of the short time for heat flow, dynamic dissolution may cause chip formation since material transport is provided by plastic flow, and diffusion is not necessary. This conclusion was supported by their microhardness data which were within the shear zones, similar to hardness of annealed material. However, microhardness of the segments was found to be the same as that of the unaffected material. It has been demonstrated that strain distribution and the depth of the deformed zone are both proportional to the depth of the indentation of the abrasive particles. Fig. 6.8 illustrates the strain distribution below worn surfaces of copper-silver solder as a function of D / ($\sigma^{1/2}$ d), which is proportional to the depth of indentation of a particle. As expected, a higher strain rate is observed at the extreme surface. High strain rates and high strains accompanied by abrasion give rise to large differences in the surface hardness and hardness profiles as a function of depth. Fig. 6.9 shows the variations of a normalised hardness as a function of depth for some steels. The alloys show significantly different profiles. This probably results from the combined effect of different processes (e.g., strain-induced phase transformation, dynamic recovery and recrystallisation, strain softening) involved during abrasion.

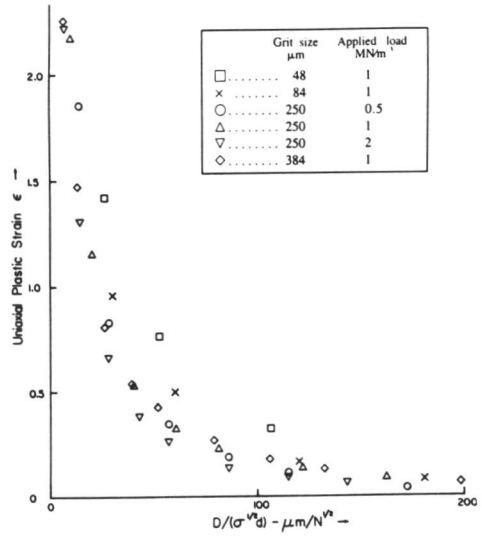

Fig. 6.8: Strain distribution below the worn surfaces of copper-silver solder as a function of $D / (\sigma^{1/2} d)$, which is proportional to the depth of indentation of a particle.[78]

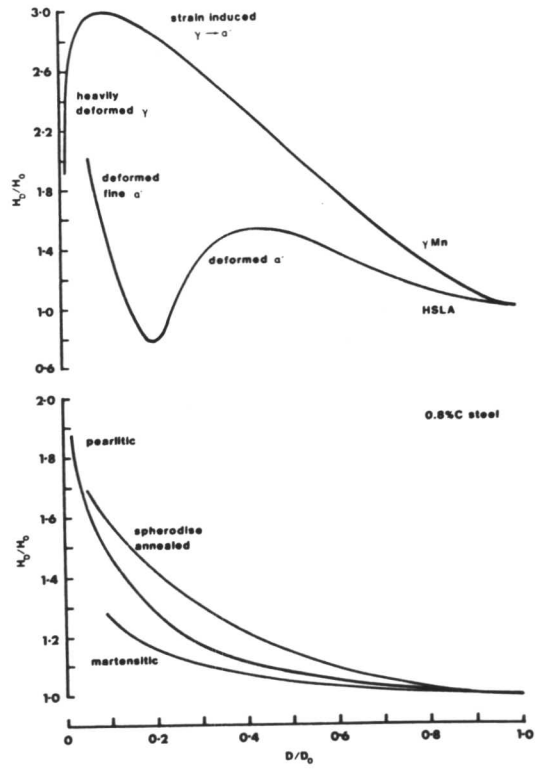

Fig. 6.9: Normalized hardness variations as a function of depth for some steels.[78]

It was shown that even under (50μm depth) work hardened layer, under some circumstances, matrix may not provide enough support to the carbides, and this leads to severe subsurface cracking and breaking fragments.[70] These results clearly indicate that subsurface deformation characteristics of the matrix phases play an important role in abrasive wear resistance. However, much more work is needed due to the complexity of this phenomenon.

So far the effect of carbides and matrix phases on wear resistance has been examined. On the other hand, it is well known that some other microstructural constituents such as inclusions, grain boundaries and internal notches have an influence as well. However, in iron-based hardfacing alloys, these parameters are not as effective as carbide and matrix phases on wear resistance.[35,46]

6.4 Effect of the Microstructure on Oxidation and Corrosion Resistance

Most of the iron-based hardfacing alloys have a poorer corrosion, and oxidation resistance than cobalt and nickel-based alloys and are therefore limited in their applications.[79] On the other hand, their low cost and good wear resistance encourages research for new iron-based hardfacing alloys as alternatives to the more expensive nickel and cobalt-based alloys. Iron-based alloys have been particularly used in applications involving the handling of abrasive slurries in gas scrubber installations used in coal-fired power stations, and for the high-speed, high-pressure pumps in coal liquefaction projects. They are used because of their good abrasive wear resistance at high temperatures at which many steels have a softening problem.[80]

Corrosion can cause substantial material loss especially during abrasion. The intense deformation and its associated dislocation activity at the abraded surfaces accelerates the corrosion rate[81,82] so that wet wear is generally worse compared with dry wear.[83] Iron-based hardfacing alloys, in applications such as track shoe materials in the water field, slurry pumps in corrosive environments (e.g. mineral and coal mines) are subjected to corrosive-abrasive and blast furnace liners for ball mills are exposed to high temperature (up to 1000^{o}C) oxidative-abrasion conditions. Also for all other applications atmospheric corrosion is inevitable.

The formation of corrosion pits is known to lead to an increase in material removal rates.[84] This phenomenon can be explained in hypereutectic alloys by the lower electrode potential of the matrix which corrodes faster than the carbides.[18] Once the matrix has corroded, its support to the carbides is weaker giving poor wear resistance. Another detrimental effect of corrosion on wear resistance is that it causes the removal of extensive corrosion products, and therefore results in high volume loss and poor wear resistance.

Since the microstructure has an influence on corrosion reactions, and especially on the distribution and path of the corrosion attack,[85] any change that retards the anodic reaction gives beneficial results. It is very well known that chromium is a key element for oxidation and corrosion resistance in steels and in iron-based alloys.[86,87] At least ≈ 12 wt%Cr is needed for good oxidation and corrosion resistance.[87] Although hypereutectic Fe-based hardfacing alloys contain up to 40 wt% Cr, the matrix itself contains much less chromium due to the high amount of Cr-rich carbides. For instance an alloy having 34%Cr and 1%C does not rust when exposed to the atmosphere in the cast structure, but as the C content increases, a rust film develops readily.[85] This is believed to occur as a result of an insufficient amount of Cr in the matrix as a consequence of Cr carbide formation. Although carbides act cathodically in a corrosion current circuit, the corroded matrix decreases its support for the carbides resulting in spalling off the carbides and poor wear resistance. It is well known that Cr-depleted regions are much more vulnerable to corrosion.[88,89] In order to increase the oxidation and corrosion resistance of Fe-Cr-C alloys the addition of other alloying elements has also been attempted. Copper is one of the most effective alloying elements which increases corrosion resistance and has been successfully used in the Cor-Ten weathering steels.[90] Cu promotes anodic passivity and forms protective corrosion

products. A similar attempt was made by Lin and Qingde[18] in cast iron containing ≈ 28%Cr, and ≈ 2.8%C by the addition of 2%Cu. They showed that M_7C_3 carbides rejected Cu during solidification and subsequently, the Cr-depleted zone around the carbides became richer in Cu which raised the electrode potential of austenite and eliminated intergranular corrosion.

Other alloying elements such as Si, Mn, Ni, and Mo have different effects in oxidation and corrosion resistance and will be discussed individually later on.

6.5 Conclusions

The literature concerning the effect of the microstructure on the abrasive wear resistance of iron-based alloys has been reviewed. The results indicate that there is no simple proportionality between abrasive wear resistance and initial hardness. However, the hardness of the worn surface is regarded as an important factor in determining the wear rate and correlates well with abrasive wear resistance. This suggests that wear resistance is a function of the maximum hardness of the work hardened surface.

Among the microstructural constituents, the hard carbides play a major role in enhancing wear resistance although their influence depends on the type of abrasives used. If the abrasives are softer than the carbides, then the latter may not deform, resulting in relatively good wear resistance. On the other hand, if the abrasives are harder than the carbides, they may deform causing subsequent cracking and spalling off carbides, giving rather poor wear resistance.

Abrasive wear resistance is also found to depend on the carbide size. There is an optimum carbide size at which carbide deformation and cracking are prevented. If the deposit cooling rate influences carbide size then it is also expected to have an indirect effect. Variations in the cooling rate can also alter the carbide volume fraction, the matrix microstructure, and therefore the abrasive wear resistance. This suggests that abrasive wear resistance of the weld deposits could be controlled to some extent, since the cooling rate depends on the welding parameters (e.g. heat input, welding speed).

Wear resistance is also affected by the carbide spacing. It increases as the mean free path between the carbides decreases. This is because finely spaced carbides support the matrix better and reduce its ability to undergo gross plastic flow. However, it should be borne in mind that too fine a carbide dispersion is undesirable due to carbide pull out during wear.

The volume fraction of carbides is a key factor influencing wear resistance. An increase in volume fraction is expected to enhance wear resistance until an optimum value is reached. The optimum value depends on process parameters, particle sizes etc. and may vary with abrasive characteristics and the type of test used. The type of abrasive will influence the deformation behaviour of the hardfacing deposit. With hard abrasives the carbides may be cut at low stresses, but may spall at high stresses so that test conditions must be considered.

Crystalline and structural anisotropy and orientation of the carbides with respect to the wear direction are all found to have an effect on wear resistance. Due to the lack of experimental evidence, a simple correlation between those variables and abrasive wear resistance is not possible.

There has been much work on the effect of the matrix microstructure on wear resistance. The results show that the abrasive wear resistance increases progressively from ferrite to pearlite, bainite and martensite. However, the contribution of the matrix is found to depend on other factors such as its hardness, toughness, and retained austenite content.

Carbide-matrix interfaces are also reported to have an influence on the strain energy release rate particularly at medium carbide volume fraction ($\approx$ 0.4-0.6) levels. Strong interfaces are needed for better wear resistance. Differences in thermal expansion coefficients between the carbide and matrix phases, and solute segregation at the interphases are detrimental factors for the initiation of the cracks.

The work hardening capacity of the matrix phase has a great influence on wear resistance, so that a generally work-hardenable austenitic matrix is preferred to a martensitic matrix due to surface hardening and due to strain-induced martensite transformation.

Although matrix anisotropy has an influence on wear resistance, any rationalisation fails because of the limited amount of available information.

Subsurface deformation properties of the matrix phase are an important factor in determining abrasion resistance. Parameters such as strain, strain rate, stress and temperature have gradients with depth and significantly influence the deformation characteristics of the alloys. These variables determine the reactions below the surface. Strain-induced phase transformations, dynamic recovery and recrystallisation, grain growth, and strain softening, are some of the consequences of abrasion. Since the relationship between the applied test conditions, alloy chemistry, and deformation mechanisms are not well established much more work is essential in order to determine subsurface deformation characteristics of the matrix phases in abrasive wear resistance.

6.6 References

1) C. P. COOKSON: Surfacing Journal, 1985, **16**, 125.
2) R. F. SMART: Surfacing Journal, 1979, **10**, 7.
3) T. S. EYRE: 'Wear Characteristics of Metals', Source Book on Wear Control Technology, ASM, 1978, p. 1-10.
4) F. BORIK: 'Metallurgy of Ferrous Materials for Wear Applications', in 'Wear Control Handbook', ASME Centennial Research Project, 1980, 327.
5) J. Y. SU, Q. D. ZHOU, AND Y. D. JIA: in Proc. Conf. 'Wear of Materials 1985', Am. Soc. Mech. Eng., New York, 1985, 621.
6) A. KAGAWA, T. OKAMOTO, K. SAITO, and M. OHTA: J. Mater. Sci., 1984, **19**, 2546.
7) F. MARATRAY, and O. USEGLIO-NANOT: 'Factors Affecting Chromium and Chromium-Molybdenum White Cast Irons', Molybdenum, Ann Arbor, USA.
8) E. RABINOWICZ: in Proc. Conf. 'Wear of Materials 1983', Am. Soc. Mech. Eng., New York, 1983, 12.
9) A. E. MILLER: 'Wear in Tillage Tools', in 'Wear Control Handbook', ASM, 1978, 987.
10) J. K. FULCHER, T. H. KOSEL, and N. F. FIORE: Wear, 1983, **84**, 313.
11) L. FANG, Q. RAO, and Q. ZHOU: in Proc. Conf. 'Wear of Materials 1987', Am. Soc. Mech. Eng., New York, 1987, 733.
12) X. KRETSCHMER: in Proc. Conf. 'Surfacing by Welding', May, 1983, 36.
13) W. WAHL: in Proc. Conf. 'Surfacing by Welding', May, 1983, 59.
14) H. BERNS, and A. FISCHER: in Proc. Conf. 'Wear of Materials 1983', Am. Soc. Mech. Eng., New York, 1983, 298.
15) J. XING, W. LU, and X. WANG, in Proc. Conf. 'Wear of Materials 1983', Am. Soc. Mech. Eng., New York, 1983, 45.
16) T. H. KOSEL, N. F. FIORE, J. P. COYLE, S. P. UDVARDY, and W. A. KONKEL: in Proc. Conf. 'Corrosion-Erosion Behaviour of Materials', St. Louis, Missouri, October 1978, Metallurgical Society of AIME, 190.
17) J. S. SUN: in Proc. Conf. 'Wear of Materials 1983', Am. Soc. Mech. Eng., New York, 1983, 79.
18) H. LIN, and Z. QINGDE: in Proc. Conf. 'Wear of Materials 1987', Am. Soc. Mech. Eng., New York, 1987, 653.
19) S. V. PRASAD, and T. H. KOSEL, in Proc. Conf. 'Wear of Materials 1983', Am. Soc. Mech. Eng., New York, 1983, 121.
20) M. A. MOORE, and F. S. KING: in Proc. Conf. 'Wear of Materials 1979', Am. Soc. Mech. Eng., New York, 1979, 275.
21) P. A. SWANSON, and R. W. KLANN: in Proc. Conf. 'Wear of Materials 1981', Am. Soc. Mech. Eng., New York, 1981, 379.
22) M. A. MOORE, and F. S. KING: in Proc. Conf. 'Wear of Materials 1979', Am. Soc. Mech. Eng., New York, 1979.
23) R. C. RICHARDSON: Wear, 1967, **10**, 353.
24) W. L. SILENCE: in Proc. Conf. 'Wear of Materials 1977', Am. Soc. Mech. Eng., New York, 1977, 77.
25) H. R. SHETTY, T. H. KOSEL, and N. F. FIORE: Wear, 1982, **80**, 347.
26) W. M. DESAI, C. M. RAO, T. H. KOSEL, and N. F. FIORE, Wear, 1984, **94**, 89.
27) S. JUNYI, and J. YUDING, in Proc. Conf. 'Wear of Materials 1987', Am. Soc. Mech. Eng., New York, 1987, 661.
28) K. H. ZUM GAHR, and D. V. DOANE: Metall. Trans. A., 1980, **11A**, 613.
29) G. G. GARRETT, G. J. WRIGHT, J. L. HENDERSON, and T. ELLIS: in first International Proc. Conf. on 'Surface Engineering', Brighton, 1985, Welding Institute.
30) R. B. GUNDLACH, and J. L. PARKS: in 'Source Book on Wear Control Technology', ASM, 1978, p. 126-131.

31) G. A. KORTELEV, M. R. NIKOLAENKO, A. N. OLISOV, and G. D. SHEVCHENKO: Welding Production, 1970, **17**, 31.
32) V. S. POPOV et al.: Welding Production, 1976, **23**, 36.
33) H. DRZENIEK, M. KOWALSKI, and E. LUGSCHEIDER: Surfacing Journal, 1985, **16**, 121.
34) K. J. BHANSALI, and W. L. SILENCE: Metal Progress, 1977, VOLUME, 39.
35) K. H. ZUM GAHR: Metal Progress, 1979, VOLUME, 46.
36) J. D. B. De-MELLO, M. DURAND-CHARRE, and T. MATHIA: Wear, 1986, **111**, 203.
37) C. E. C. RENSE, G. R. EDWARDS, and H. R. FROST: J. Materials for Energy Systems, 1983, **5**, 149.
38) D. N. NOBLE: Met. Con., 1985, **17**, 605.
39) K. H. ZUM GAHR: in Proc. Conf. 'Wear of Materials 1985', Am. Soc. Mech. Eng., New York, 1985, 45.
40) J. XING, W. LU, and X. WANG: in Proc. Conf. 'Wear of Materials 1983', Am. Soc. Mech. Eng., New York, 1983, 45.
41) F. BORIK, and J. C. MAJETICH: in Proc. Conf. 'Wear of Materials 1985', Am. Soc. Mech. Eng., New York, 1985, 595.
42) K. H. ZUM GAHR, and G. T. ELDIS: Wear, 1980, **64**, 175.
43) D. N. NOBLE: 'The Effect of Flux-Cored Arc Welding Conditions on Microstructure and Abrasive Wear Resistance of Two Iron-Based Hardfacing Alloys', Welding Institute Research Report, 7856.02/86/479.3, November, 1986.
44) D. H. BUCKLEY, and E. RABINOWICZ: 'Fundamentals of the Wear of Hard Materials', in 2nd Int. Proc. Conf., 'Science Hard Materials', 1986, 825.
45) V. V. TARASOV et al.: Welding Production, 1976, **23**, 33.
46) K. H. ZUM GAHR: in Proc. Conf. 'Wear of Materials 1979', Am. Soc. Mech. Eng., New York, 1979, 266.
47) D. E. DIESBURG, and F. BORIK: 'Optimizing Abrasion Resistance and Toughness in Steels and Irons for the Mining Industry', in Source Book on Wear Control Technology, ASM, 1978, p. 94-113.
48) R. J. DAWSON, J. E. PRITCHARD, and R. A. BELAND: in Proc. Conf. 'Wear of Materials 1983', Am. Soc. Mech. Eng., New York, 1983, 97.
49) N. J. KAR:in Proc. Conf. 'Wear of Materials 1981', Am. Soc. Mech. Eng., New York, 1981, 415.
50) P. L. HURRICKS: Wear, 1973, **26**, 285.
51) C. K. KWOK, and G. THOMAS: in Proc. Conf. 'Wear of Materials 1983', Am. Soc. Mech. Eng., New York, 1983, 140.
52) H. K. D. H. BHADESHIA, and D. V. EDMONDS: Part I, metal Science, 1983, **17**, 411.
53) W. J. SALESKY, and G. THOMAS: in Proc. Conf. 'Wear of Materials 1981', Am. Soc. Mech. Eng., New York, 1981, 298.
54) K. H. ZUM GAHR: Z. Metallkd., 1977, **68**, 783.
55) N. F. FIORE, J. P. COYLE, S. P. UDVARY, T. H. KOSEL, amd W. A. KONKEL: Wear, 1980, **62**, 387.
56) T. H. KOSEL, and N. F. FIORE: J. Materials for Energy Systems, 1981, **3**, 7.
57) K. H. ZUM GAHR: Z. Metallkd., 1980, **71**, 103.
58) C. KIM, A. PATTNAIK, and R. J. WEIMER: in Proc. Conf. 'Mechanical Behaviour of Metal-Matrix Composites', Metallurgical Society of AIME, 1982, pp. 95-116.
59) D. L. DAVIDSON, R. M. ARROWOOD, J. E. HACK, G. R. LEVERANT, and S. P. CLOUGH: in Proc. Conf. 'Mechanical Behaviour of Metal-Matrix Composites', Metallurgical Society of AIME, 1982, p. 117-142.
60) V. M. ERSHOV: Chernaya Metall (Eng. Trans.), 1984, **8**, 101.

61) L. E. MURR: 'Interfacial Phenomena in Metals and Alloys', 1975.
62) A. S. ARGON, J. IM: Metall. Trans. A., 1975, **6A**, 825.
63) A. S. ARGON, J. IM., and R. SAFOGLU: Metall. Trans. A., 1975, **6A**, 825.
64) G. T. HAHN, M. F. KANNINEN, and A. R. ROSENFIELD: 'Annual review of Materials Science', 1972, **2**, 381.
65) M. YOSHIDA, and H. SUTO: J. Jpn. Inst. Met., 1979, **43**, 433.
66) M. YOSHIDA: Scripta Metallurgica, 1982, **16**, 787.
67) S. S. IBRAGIMOV, A. M. IL'IN, V. V. ZASHKVARA, and E. A. TKACHENKO: Poverkhnost Fizika Khimiia Mekanika, 1983, **12**, 72.
68) H. GLEITER: in Proc. Conf. 'Structure and Properties of Internal Interfaces', August 1984, 333.
69) A. M. EL-RAKAYBY, and B. MILLS: Wear, 1986, **112**, 327.
70) J .T. H. PEARCE: Wear, 1983, **89**, 333.
71) S. SHEPPERSON, and C. ALLEN: in Proc. Conf. 'Wear of Materials 1987', Am. Soc. Mech. Eng., New York, 1987, 573.
72) U. R. LENEL, and B. R. KNOTT: in Proc. Conf. 'Wear of Materials 1987', Am. Soc. Mech. Eng., New York, 1987, 635.
73) E. HORNBOGEN:in Proc. Conf. 'Wear of Materials 1985', Am. Soc. Mech. Eng., New York, 1985, 477.
74) N. P. VASIL'EV: Welding Production, 1980, **27**, 27.
75) U. HEROLD-SCHMIDT, and R. HINSBERGER: in Proc. Conf. 'Wear of Materials 1987',Am. Soc. Mech. Eng., New York, 1987, 565.
76) G. E. DIETER: Mechanical Metallurgy, 2nd Edition, 1981, 356.
77) S. SODERBERG, U. BRYGGMAN, and A. CANALES: Wear, 1985, **105**, 1.
78) M. A. MOORE: 'Abrasive Wear', in 'Fundamentals of Friction and Wear of Materials', ASM Materials Science Seminar, 1980, 73.
79) Metalls Handbook, Vol. 8, American Society for Metals, Ohio, USA, 1973.
80) J. DODD: J. Materials for Energy Systems, 1980, **2**, 65.
81) R. J. NOEL, and A. BALL: in Proc. Conf. 'Wear of Materials 1983', Am. Soc. Mech. Eng., New York, 1983, 148.
82) K. Y. KIM, S. BHATTACHARYYA, and V. AGARWALA: in Proc. Conf. 'Wear of Materials 1981', Am. Soc. Mech. Eng., New York, 1981, 772.
83) C. ALLEN, B. E. PROTHEROE, and A. BALL: in Proc. Conf. 'Wear of Materials 1981', Am. Soc. Mech. Eng., New York, 1981, 271.
84) P. ZHOU, J. SUN, and X. ZHANG: in Proc. Conf. 'Wear of Materials 1983', Am. Soc. Mech. Eng., New York, 1983, 87.
85) P. W. BROWN, and L. W. MASTERS: 'Factors Affecting the Corrosion of Metals in the Atmosphere', in 'Atmospheric Corrosion', Ed. W. H. AILOR, 1982, 31.
86) R. A. PACEY: 'Hardfacing and the Role of Chromium', Chromium Review, 1985, **5**, 32.
87) M. J. JOHNSON, and P. J. PAVLIK: 'Atmospheric Corrosion of Stainless Steel', in 'Atmospheric Corrosion', Ed. W. H. AILOR, 1982, 461.
88) "Corrosion Engineers", M. G. FONTANA, and N. D. GREENE: 2nd. edition, Mc-Graw Hill Series in Materials Science and Engineering, 1978, pp. 59-60.
89) L. M. GRIBAUDO, M. D. CHARRE, and S. THIBAULT: J. of Materials Science, 1985, **20**, 1983.
90) I. L. ROZENFELD: 'Atmospheric Corrosion of Metals', English Language Edition by E. C. Greco, 1972.

7. MICROSTRUCTURE, ABRASIVE WEAR RESISTANCE AND STABILITY OF IRON-BASED HARDFACING ALLOYS

7.1 Introduction

As discussed previously, Fe-Cr-C type hardfacing alloys are widely used because of their low cost and good wear resistance. High chromium and high carbon concentrations (up to 40wt%Cr and 6wt%C) provide large volume fractions of carbides which in turn are believed to impart the necessary abrasive wear resistance. However, there is a large stimulus to develop new iron-based hardfacing alloys in order to achieve better properties while using cheaper and more effective alloy additions. Although there are many hardfacing alloys, only a small amount of work has been carried out towards understanding the influence of microstructure on abrasive wear resistance. Discrepancies between experimental results have been so profuse as to make the task of reaching general conclusions impossible. One of the possible reasons for the occurrence of these discrepancies is the absence of a standard wear test. Due to the differences between experimental techniques, comparison is poor and therefore the interpretation of results can be controversial.

This chapter aims to undertake a more systematic and quantitative approach towards assessing the effects of microstructure on the abrasive wear resistance and stability of the matrix and other phases.

7.2 Fe-Cr-C System

7.2.1 Experimental Technique

The microstructural characteristics and abrasive wear resistance of the alloy 78 (Fe-37.87Cr-4.50C-1.41Mn-0.86Si wt%) are discussed here. This alloy was deposited by the manual metal arc (MMA) welding technique. The weld was deposited in three layers in order to prevent a high degree of dilution, and to avoid the effects of thermal expansivity differences between the base plate and the alloy. 4mm diameter electrodes were used, the welding conditions being 160A, 23V A.C., with a welding speed of about 0.004m/s and an interpass temperature of about 350^{o}C. Thin foil specimens for transmission electron microscopy were prepared by spark machining from the top layer of the weld deposit. The thin foil preparation and microanalytical techniques are as outlined in Chapter 10. More than 15 microanalysis determinations were carried out for each phase. The following carbon corrections for the austenite were made;

if N_i is the number of atoms of elements i, with i=1 for carbon, then Y_i can be defined as follows;

$$Y_i = 100N_i / \frac{n}{2} \sum (N_i) = 1/2\ N_i \qquad .....(1)$$

Y_i thus represents the concentration of elements "i" in atomic percent when the presence of carbon is ignored. It is necessary to define such a concentration because the microanalysis technique used is not capable of recording light elements such as carbon. Then the true concentration, V_i in atomic percent is given by the following equation

$$V_i = 100N_i / \sum_{1}^{n} N_i = 100N_i / (200 + N_1) \qquad .....(2)$$

by substituting N_i into equation 2, we get

$$V_i = 200Y_i / (200 + N_1) \qquad .....(3)$$

V_C can be deduced from the lattice parameter of austenite a_o which is measured using X-ray diffractometry and concentrations of substitutional alloying elements which are known from the microanalysis experiments (assuming that the effect of carbon on these values is negligible). The lattice parameter of austenite is given by Dyson and Holmes[1] as;

$a_o(0.0021\bar{+}) = 3.5770 + 0.0065C + 0.001Mn + 0.0006Cr - 0.0002Ni + 0.0053Mo + 0.0079Nb + 0.0032Ti + 0.0017V + 0.0057W$ (at%).

and V_C and N_C are written as follows;

$$V_C = 100N_C / (N_C + 200) \qquad .....(4)$$

$$N_C = 200V_C / (100 - V_C) \qquad .....(5)$$

Since N_C is calculated as above, in general case the true concentration of alloying elements V_i is written as follows:

$$V_i = Y_i (1 - (V_C / 100)) \qquad .....(6)$$

The carbon correction for the carbides is carried out assuming stoichiometry, as explained by Svensson et al.[2]

Abrasion wear tests (pin-on-disc) were performed on 5mm diameter cylindrical specimens impinging vertically on a rotating disc coated with the appropriate abrasive. The specimens were gravity loaded with a mass of 450g or 1000g. The cylindrical samples were spark-machined from the weld deposits, so that the test surface was parallel to the layers of hardfacing material.

The weight loss due to abrasive wear was measured at various intervals during the test period. The displacement resulting from the reduction in its length was also recorded by means of a linear displacement transducer. A general photograph of the pin-on-disc abrasive wear tester and its components is shown in Fig. 7.1.

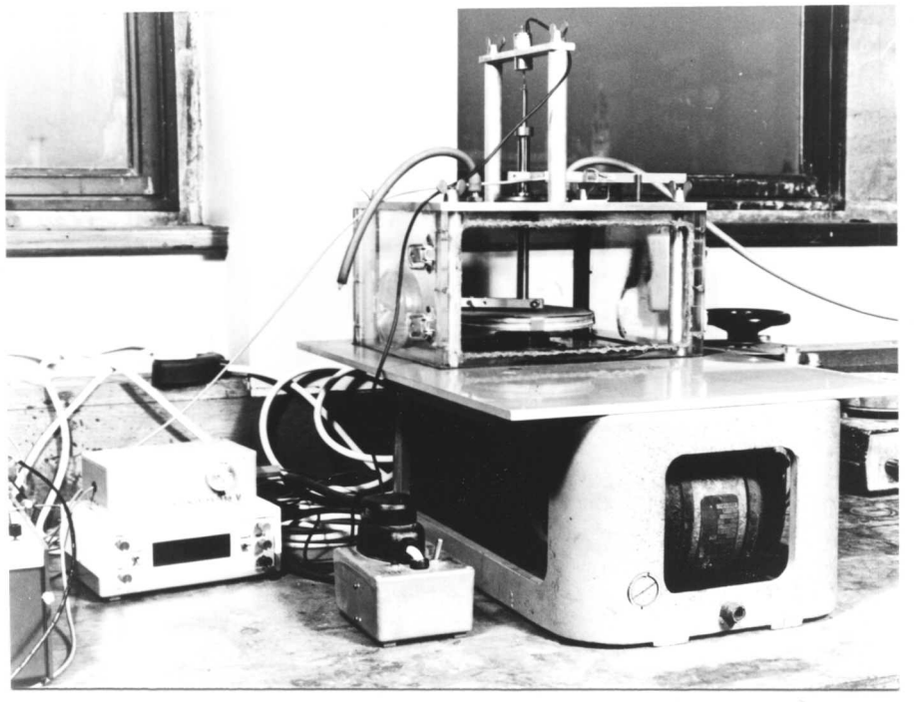

a

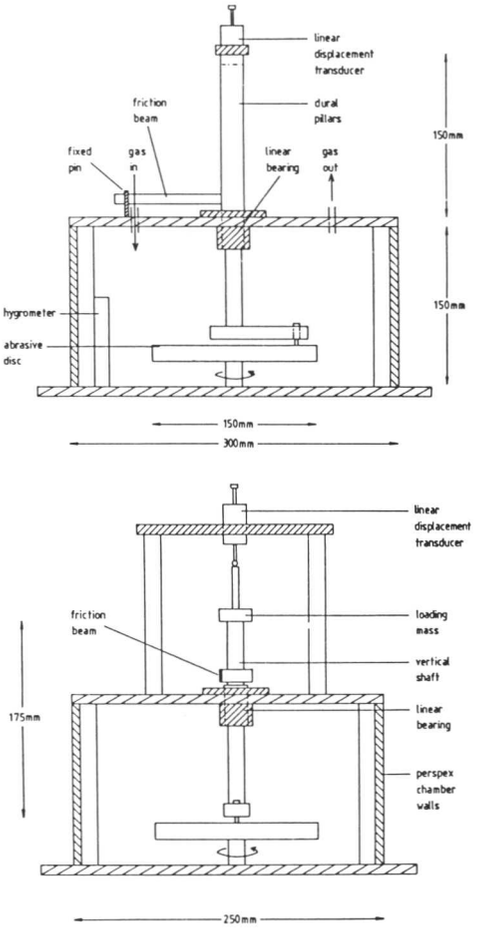

b

Fig. 7.1: a) The pin-on-disc abrasive wear tester; b) dimensions and identifications of the components of the apparatus. After Mercer.[3]

The effects of two kinds of abrasives were studied using the rotating coated-disc test: 280 mesh SiC, and 400 mesh Al_2O_3 with nominal particle sizes ≈40 and ≈17 μm respectively (Fig. 7.2). The relative velocity of the disc and sample was 0.63 m/s. In order to avoid spurious effects due to the degradation of the abrasives during the wear tests, the abrasive paper was changed at 3 minute intervals.

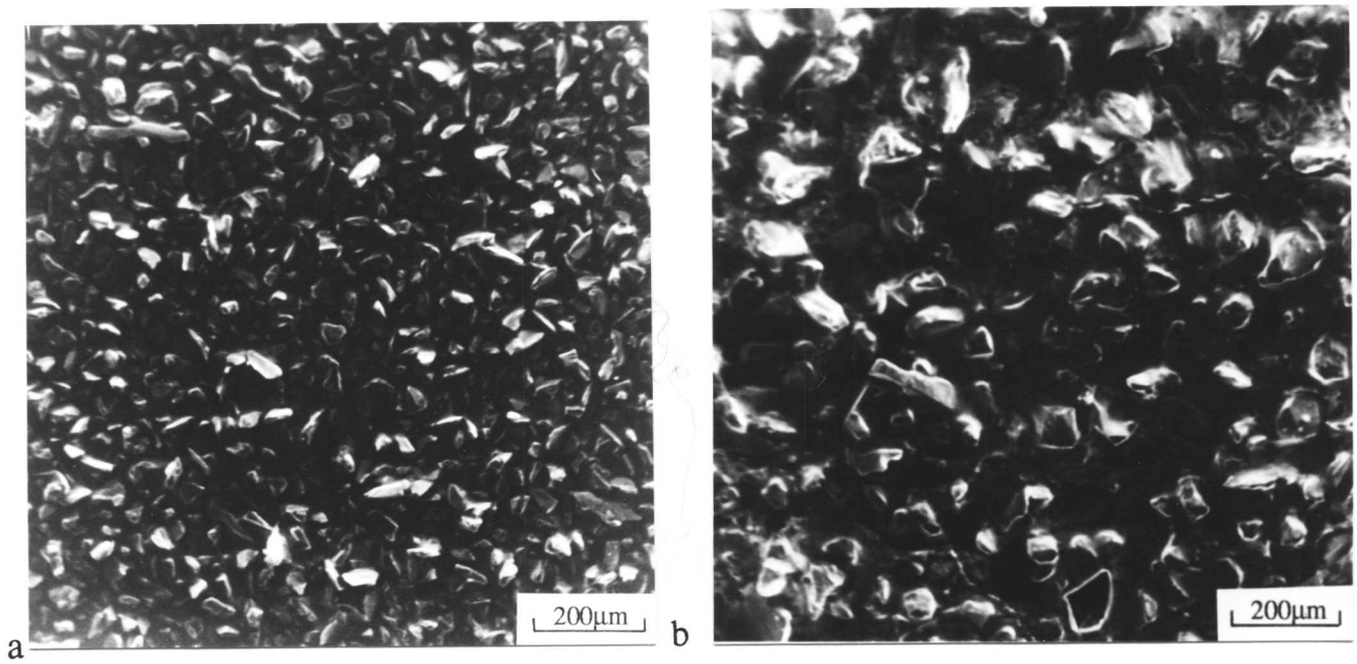

Fig. 7.2: Scanning electron micrographs of the abrasive papers used in this work; a) 400 mesh Al_2O_3; b) 280 mesh SiC.

In addition to the pin-on-disc tests, single and multiple scratch tests were carried out using a Vicker's pyramidal diamond loaded at 500 and 1000g. The scratch tool was in each case mounted at the end of a balanced parallelogram-arm instrumented with strain gauges and loaded by gravity. The specimen was then moved linearly by a geared electric motor at a speed of $0.25mms^{-1}$ for a distance of 7mm. The scratch tester, its dimensions and identification of the components are illustrated in Fig. 7.3. The worn surfaces were examined before and after the ultrasonic cleaning and then examined using a scanning electron microscope.

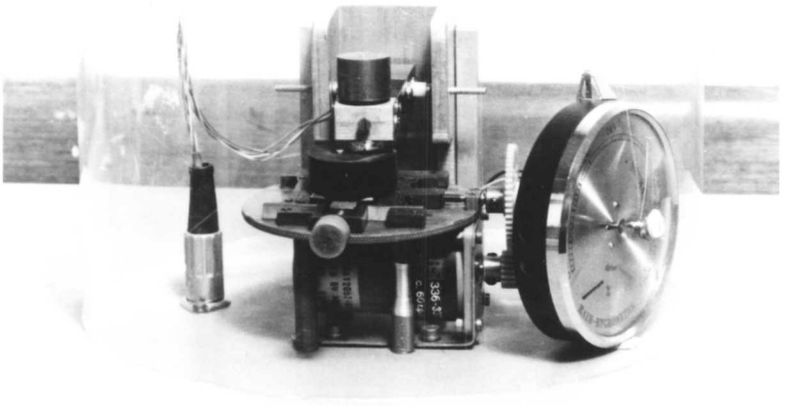

50mm

a

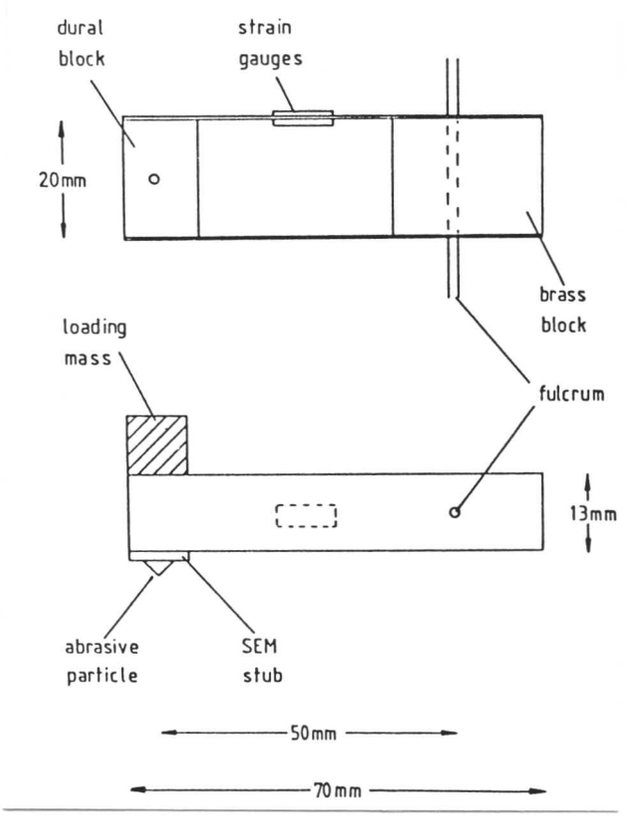

b

Fig. 7.3: a) A general photograph of the scratch tester; b) its dimensions and identification of the components; i) upper plan, ii) lower plan. After Mercer.[3]

7.2.2 Results and Discussion

If the effects of Mn and Si are ignored, the liquidus projection (Fig. 7.4) of the Fe-Cr-C system for alloy 78 indicates that primary M_7C_3 carbides are the first to precipitate in the liquid, followed by solidification as a eutectic reaction resulting in austenite and more M_7C_3 eutectic carbides, as shown in isothermal phase diagrams (Fig. 7.4b-d). However, due to high levels of dilution the microstructure is found to be of a hypoeutectic type in the first layer, containing primary austenite dendrites (Fig. 7.5a). A carbon-enriched zone in the substrate near the first layer/base metal interface suggests that a substantial amount of carbon diffuses from the cladding material into the substrate. Carbon diffusion is probably most significant when the molten metal is in contact with the substrate, because, the diffusion coefficient of carbon in the liquid iron is much higher than that of in the austenite.[4] The major growth direction of the dendrites was generally found to be perpendicular to the first layer/base metal interface due to the maximum thermal gradient in this direction.[1] Martensite formation is apparent along the substrate/first layer interface (Fig. 7.5b) where the high dilution makes the austenite unstable to such decomposition during quenching. The microstructure of the undiluted top layer was found to be consistent with the liquidus projection of the Fe-Cr-C system, showing large primary M_7C_3 carbides (Fig. 7.5c). These carbides were found to be surrounded by precipitate-free-zones. Svensson et al.[2] suggested that precipitate free zones occur due to Cr depletion of the liquid in the vicinity of the primary carbides. This has been confirmed in the present work since the Cr concentration was found to be the same in this area, as in the austenite of the eutectic mixture, implying that the former is not supersaturated with respect to the carbide phase. These primary carbides grow initially by taking the solute from the liquid and/or matrix until the matrix reaches its equilibrium composition.

---

1 The maximum thermal gradient is always normal to the solid/liquid interface. The major growth direction is <100> in the case of face-centred-cubic (fcc) crystals.[5]

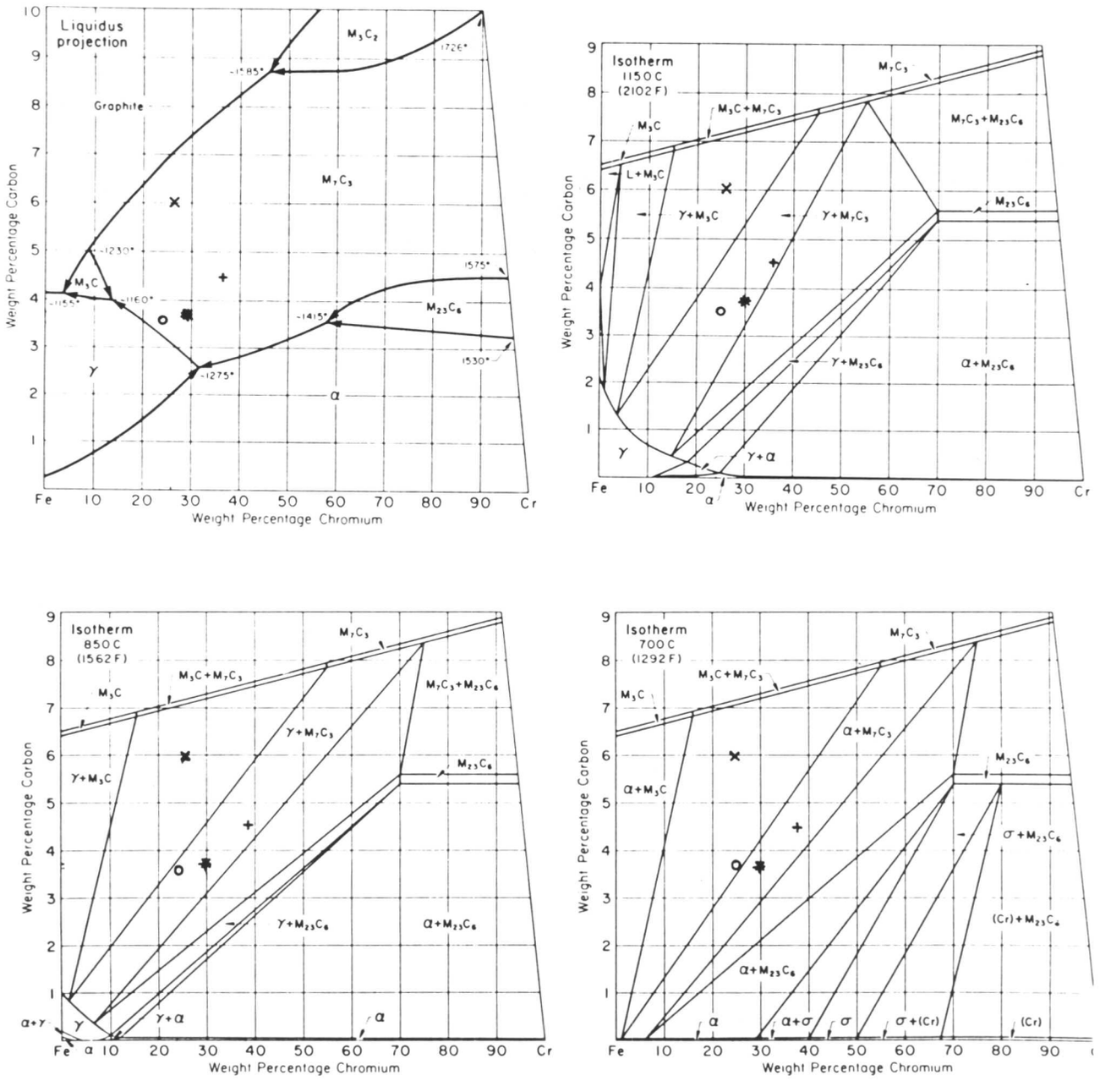

Fig. 7.4: Liquidus projection and isothermal sections of Fe-Cr-C system.[6] The points indicated on the diagram show the positions of the experimental alloys.

+ Alloy 78

o Alloy 79

x Alloy 37

* Dilatometric specimen.

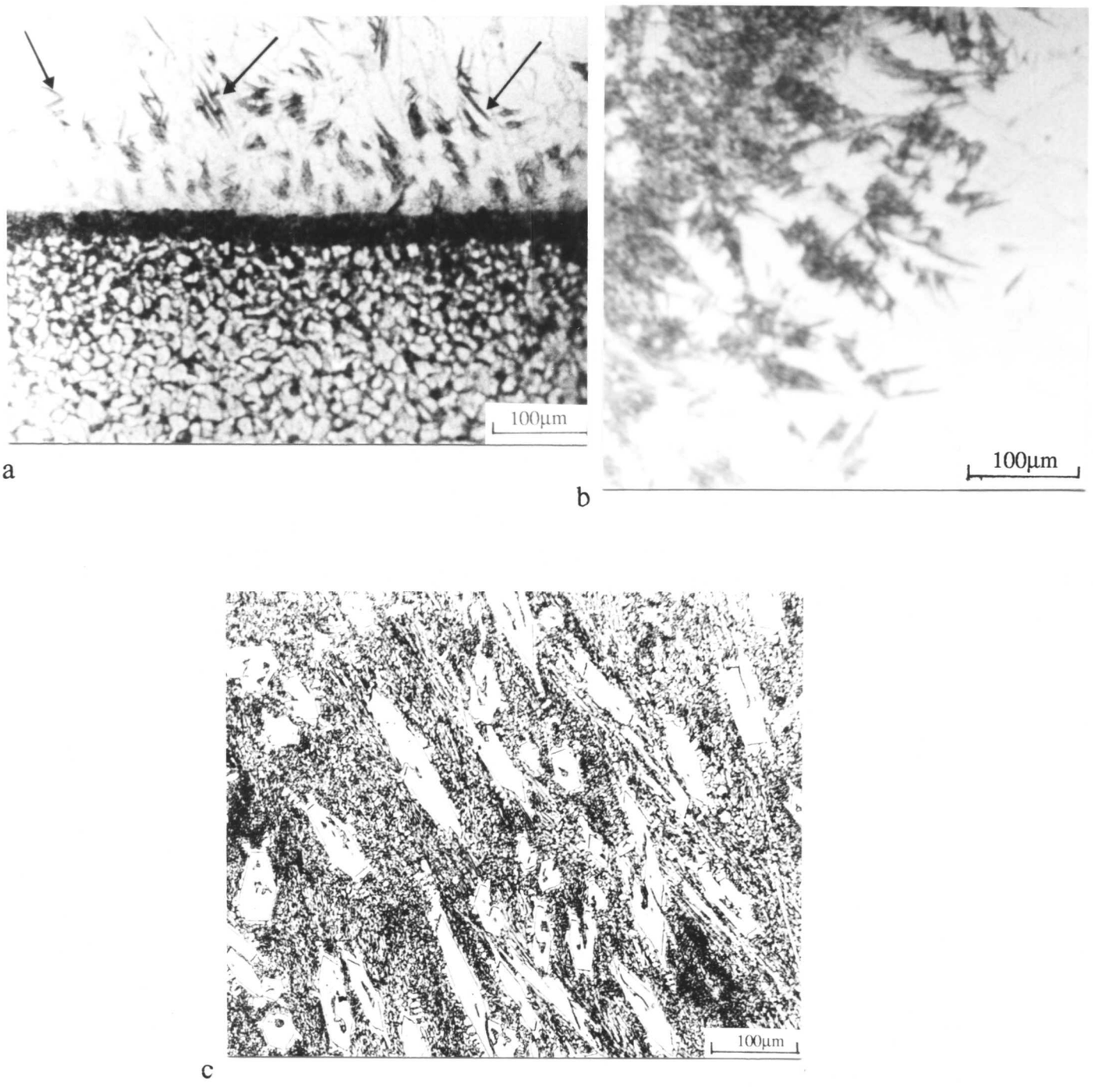

Fig. 7.5: Optical micrographs of the alloy 78 (Fe-37.87Cr-4.5C-1.41Mn-0.86Si wt%), a) cross-section showing the highly-diluted first layer/base metal interface region, the carbon enriched area in the substrate along the boundary, and dendritic solidification of the first layer clad material; b) higher magnification image showing lenticular martensite observed along the first layer/base metal interface; c) the top layer consisting of large M_7C_3 carbides surrounded by precipitate free zones and the austenitic matrix with more eutectic M_7C_3 carbides.

Transmission electron microscopy (TEM) and X-ray diffractometry results showed that the eutectic matrix contains austenite and M_7C_3 carbides (Fig. 7.6) although the equilibrium microstructure is a mixture of ferrite and M_7C_3 carbides below 700°C (Fig. 7.4d). This metastable microstructure arises due to the high cooling rates involved in the MMA welding technique (typically 20-30 K/s[2]).

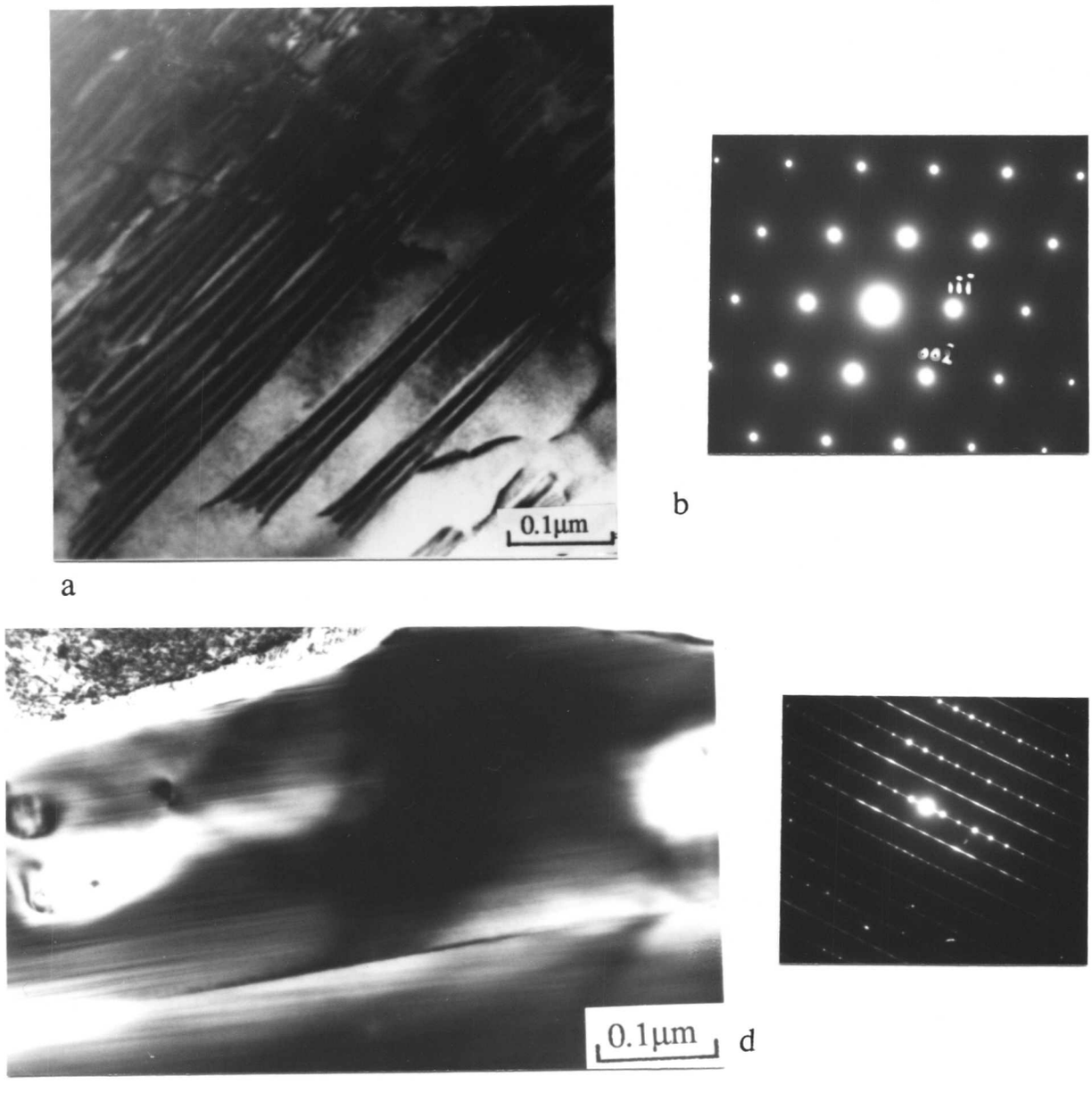

Fig. 7.6: a) Transmission electron micrograph of the austenitic matrix showing stacking faults; b) corresponding $<011>_{fcc}$ electron diffraction pattern; c) transmission electron micrograph of the M_7C_3 carbides; d) corresponding $<11.1>_{hcp}$ electron diffraction pattern.

Furthermore, the experimentally measured γ/M_7C_3 partition coefficient of chromium was found to be 3.5, which indicates that the structure is configurationally frozen around 1100°C (Fig. 7.7).[2] Since the melting temperature of the alloy is around 1380°C, the entire microstructure could be considered to have formed within the temperature range of 1380-1100°C.

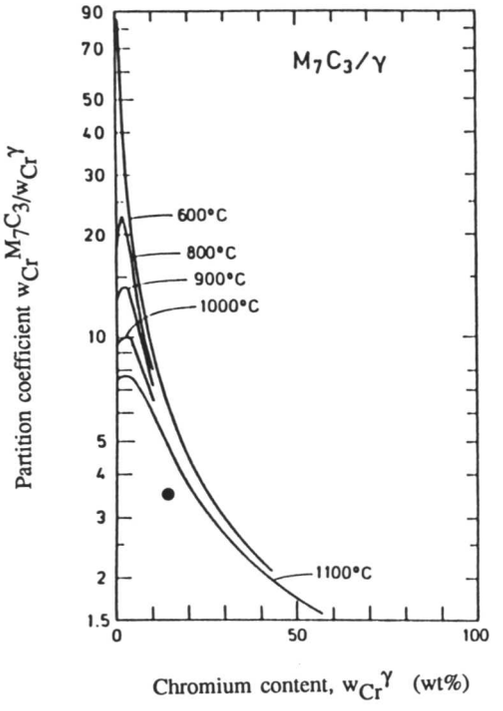

Fig. 7.7: Variation of the γ/M_7C_3 partitioning coefficient of chromium as a function of temperature.[8] The point shows the experimentally calculated partition coefficient of Cr, indicating that the microstructure is configurationally frozen around 1100°C.

2 A *configurationally frozen* microstructure is one which does not change during cooling from the temperature at which it becomes configurationally frozen[7]. The term *frozen* is not to be confused with the freezing of liquid. In the present context, the alloy solidifies and then becomes configurationally frozen at some lower temperature where the mobility of atoms becomes inadequate, for the given cooling rate, to support diffusional transformation. It should be noted that a higher cooling rate should increase the temperature at which a microstructure becomes configurationally frozen.

The remaining microstructure consists of fine eutectic M_7C_3 carbides in the austenitic matrix as confirmed by TEM and X-ray diffractometry (Fig. 7.6, Table 7.1). Microanalysis results (Fig. 7.8) showed that the M_7C_3 carbides are $(Fe,Cr)_7C_3$ type carbides, consistent with the fact that M_7C_3 is known to dissolve up to 55wt% Fe[6]. The results also indicate that Mn preferentially partitions into the carbide phase and Si is rejected by the carbides. The crystal structure of M_7C_3 carbides is discussed in detail in Chapter 10.

TEM results showed that the matrix is fully austenitic and contains a high density of stacking faults (Fig. 7.6). The faulting is promoted by Cr, which lowers the stacking fault energy (SFE) of austenite and increases the stacking fault probability.[9]

Microanalytical results (Fig. 7.8, Table 7.2) showed that the austenite contains ≈16.6Cr at%. This is slightly above the critical value[3] of Cr required to form a uniform Cr_2O_3 oxide layer for good oxidation and corrosion resistance. However, at service temperatures below 700°C, the austenitic matrix is expected to transform to ferrite and more M_7C_3 carbides, the ferrite having a much lower Cr content. This obviously will decrease the oxidation and corrosion resistance of the alloy. The implications of the austenite-to-ferrite transformation and its significance on oxidation and corrosion resistance, and wear resistance will be discussed later.

Scanning electron micrographs of the worn surfaces after the pin-on-disc abrasion test using SiC (220 mesh) at 1kg and Al_2O_3 (400 mesh) abrasives at 450g load revealed that the abrasive particles cut the primary carbide phase (Fig. 7.9). Also, there is no marked indication of any change in the width of the groove as it passes from the matrix to carbide phases. These results indicate that the carbides are worn almost to the same level as the matrix (eutectic mixture) under these test conditions. Furthermore, carbide cracking and pit formation along the carbide-matrix interface (Fig. 7.9) suggests that the interfaces are vulnerable to cracking probably due to high stress concentrations in these regions. The debris particles around the pits were examined before ultrasonic cleaning, using energy-dispersive-X-ray analysis. The results showed that these particles contain a high amount of Cr, implying that these are Cr-rich M_7C_3 type carbide fragments. It is a fact that carbide/matrix interfaces have a significant influence on strain energy release and crack propagation during abrasion. The strain energy is released much faster at the carbide/matrix interfaces at medium carbide volume fractions (≈ 0.3-0.6)[11] than the other phases (e.g. matrix, carbides) giving rise to a decrease in wear resistance. It is possible that the carbide fragments may behave as abrasive particles themselves leading to a higher weight loss.

---

3 Minimum Cr concentration is suggested to be at least 12wt% for good oxidation and corrosion resistance.[10]

Table 7.1: X-ray diffractometry results; d spacings and corresponding Miller indices of present phases in Alloy 78.

d (Å)	hkl
2.28	$24.0_{M_7C_3}$
2.076	111_{γ}
2.032	$24.1_{M_7C_3}$
1.807	002_{γ}
1.746	$442_{M_7C_3}$
1.274	220_{γ}
1.168	$01.1_{M_7C_3}$
1.088	$47.2_{M_7C_3}$
1.042	222_{γ}

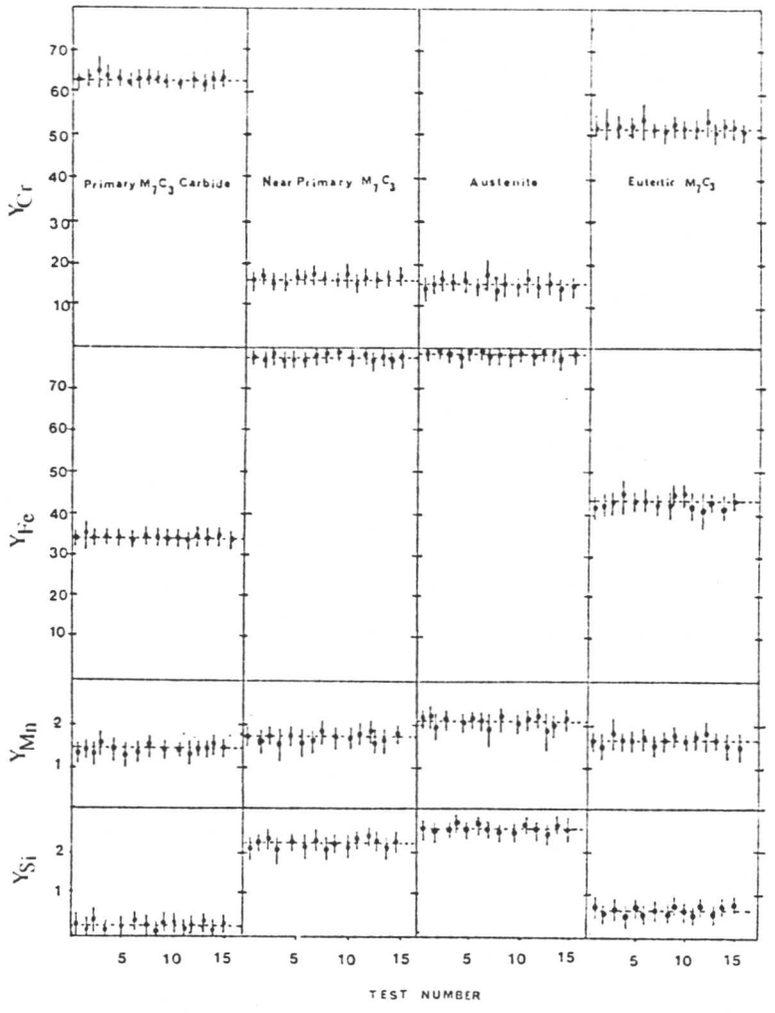

Fig. 7.8: Microanalytical data on primary M_7C_3, eutectic M_7C_3, near primary M_7C_3, and austenitic matrix, when C is not included (continuous lines show the average values in each phase) at%.

Table 7.2: Mean compositions of the phases. The results are quoted to three decimal places for internal consistency; typical error bars are illustrated in Fig. 7.8. The results for the primary carbides, and for the austenite near the primary carbides (Near P. Carbide) are obtained using scanning electron microscopy.

	Primary Carbide		Near P. Carbide		Austenite	
	Y_i	V_i	Y_i	V_i	Y_i	V_i
Fe	33.050	23.140	78.710	76.133	78.750	76.170
Cr	65.240	45.680	17.350	16.780	16.620	16.070
Mn	1.490	1.043	1.740	1.683	2.050	1.982
Si	0.220	0.154	2.200	2.128	2.580	2.490
C		30		3.273		3.273

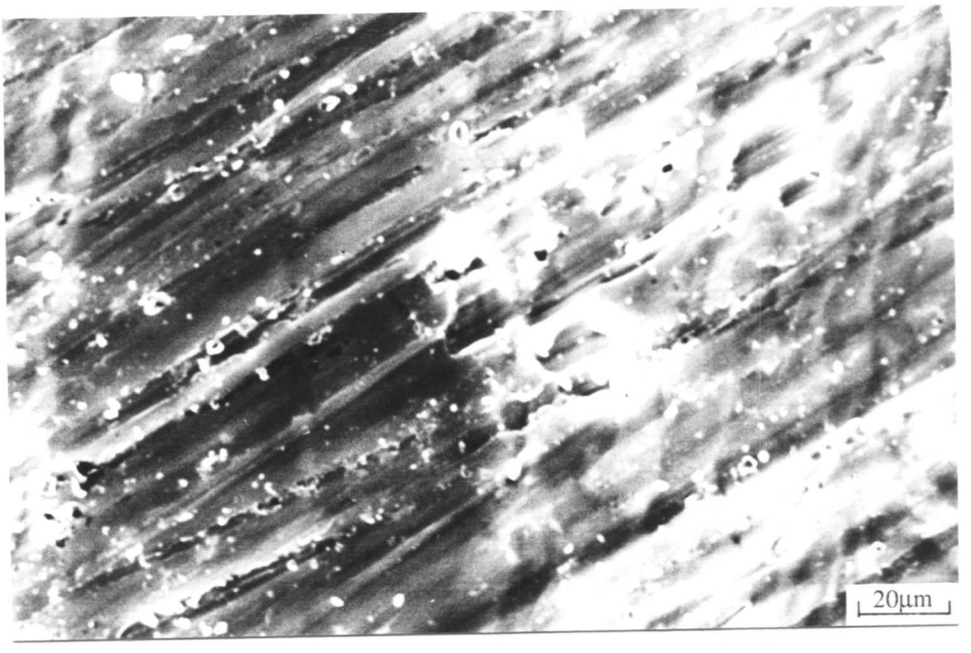

a

b

Fig. 7.9: Scanning electron micrographs of the worn surfaces of alloy 78 after the pin-on-disc abrasion test using; a) SiC (220 mesh) abrasives at 1kg load showing that carbides are worn to the same level as the matrix; b) Al_2O_3 (400 mesh) at 450g, showing pit formation along the carbide-matrix interface.

Single-pass-scratch test results at 500g and 1kg, using the Vickers pyramid scratch tool, show that there is almost no difference in the scratch groove dimension for the carbide and matrix phases (Fig. 7.10). Carbide cracking is also apparent at the two different loads. However, it is more apparent with the higher load (Fig. 7.10). These cracks were found almost to be perpendicular to the scratch groove direction. Also, it is clear that the matrix phase with eutectic carbides are ploughed to both sides of the groove (Fig. 7.10). This suggests that the fine eutectic carbides are entirely removed within the scratch.

Single-pass-scratch test and pin-on-disc abrasion test results indicate that the carbides do not increase the abrasive wear resistance under heavy abrasive wear conditions. They cannot resist being cut out by abrasives, and the carbide/matrix interfaces are extremely vulnerable to cracking and spalling.

7.2.3 Conclusions

The top layer (undiluted) microstructure of alloy 78 (Fe-37.87Cr-4.5C-1.41Mn-0.86Si wt%) was found to consist of primary M_7C_3 carbides in the eutectic mixture of austenite and M_7C_3 carbides. Microanalytical results showed that the as-deposited microstructure is configurationally frozen at about 1100°C. This metastable microstructure arises due to high cooling rates involved in the manual metal arc welding technique, and given sufficient thermal activation, the austenite should transform to chromium poor ferrite and more M_7C_3 carbides. Such a decrease in chromium level is expected to be detrimental to oxidation and corrosion resistance of these alloys.

Abrasive wear test experiments using SiC and Al_2O_3 abrasives showed that the carbides wear to the same level as the matrix phase. Extensive carbide cracking is observed. The cracks were found to stop at the carbide/eutectic mixture interfaces. This is because the strain associated with the deformation is relaxed into the matrix phase. Pits along the carbide/matrix interfaces were observed extensively indicating that the interfaces are vulnerable to cracking probably due to high stress concentrations in these regions.

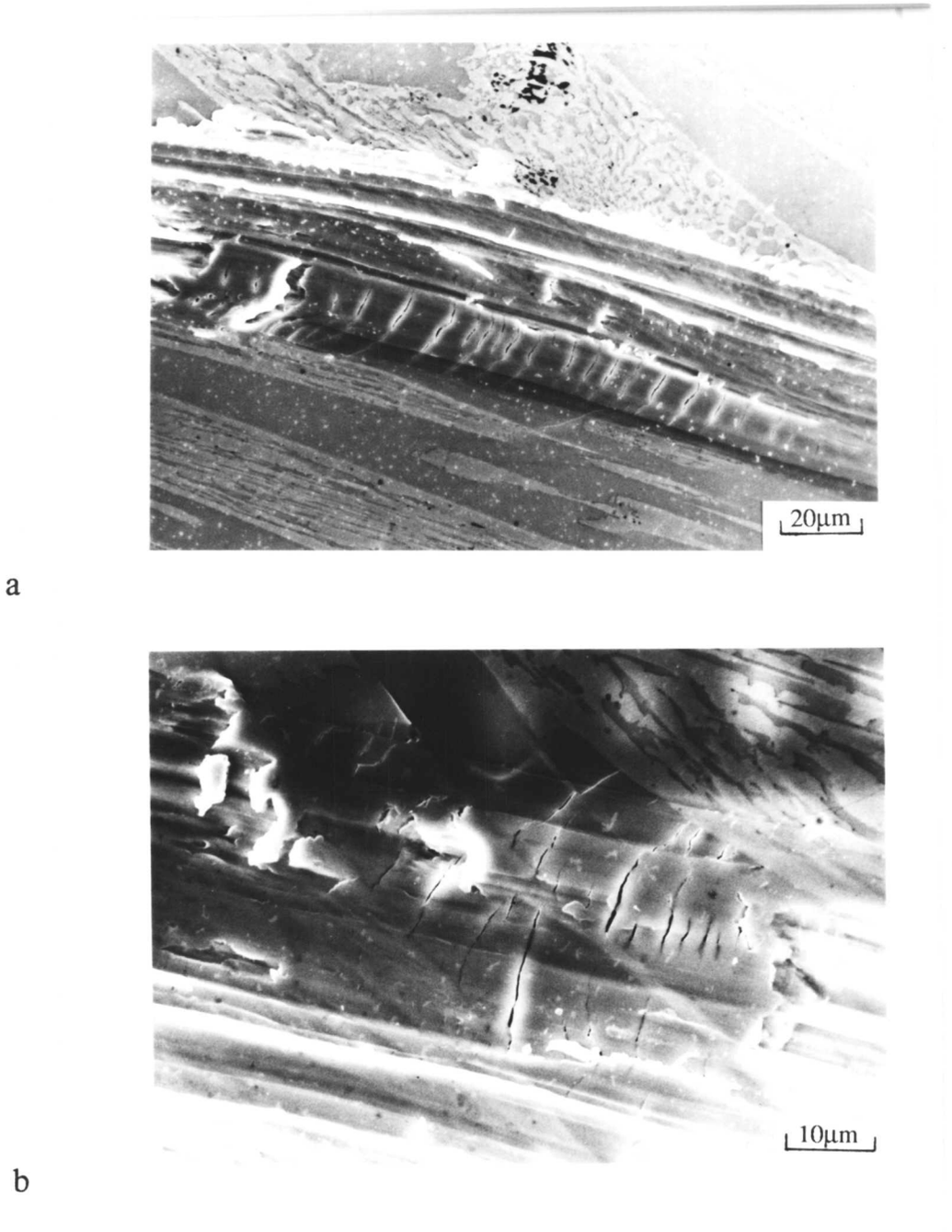

Fig. 7.10: Scanning electron micrographs after single-pass scratch tests; a) at 500g b) at 1kg, showing carbide cracks which stop at the carbide/eutectic interfaces since the deformation is released into the matrix phase at these regions.

7.3 Transformation of Austenite

7.3.1 Introduction

The microstructural characteristics of the Fe-Cr-C hardfacing Alloy 78 were discussed in the last section. The microstructure was found to contain metastable austenite which should transform to ferrite and more M_7C_3 carbides at extended service temperatures (below 700°C). The ferrite is expected to have a much lower chromium concentration. Hence, although transformation may not significantly influence the wear properties of these alloys the oxidation and corrosion resistance are expected to deteriorate. Therefore, the kinetics of this transformation and the properties of the subsequent microstructure have to be understood.

7.3.2 Experimental Technique

The transformation of austenite was studied in a Fe-29.19Cr-3.80C-1.32Mn-0.59Si-0.01Mo (wt%) alloy deposited by the manual metal arc welding technique. Due to the difference in chemical composition with Alloy 78, microanalysis experiments were carried out as explained in the last section. Specimens for dilatometric experiments were machined from the top layer of the weld deposit. The specimens were nickel-plated in order to prevent any surface nucleation and/or surface degradation effects. Nickel plating was carried out in two stages; striking and plating. Striking was carried out in a solution containing 250g $NiSO_4$, 27ml conc. sulphuric acid, and water, ammounting to 1 litre in all at 50°C. The plating solution is made up of 140g $NiSO_4$, 140g anhydrous sodium sulphate, 15g ammonium chloride, and 20g boric acid, made up to 1 litre with distilled water. The plating was carried out at 50°C, with a current density of ≈50mA/cm^2 for 15 minutes. The dilatometer has been specially interfaced with a BBC/ACORN microcomputer so that length, time and temperature variations can be recorded and stored at a rapid rate. The relative length change ($\Delta L/L$) during isothermal transformation was measured and the corresponding length change versus time curve plotted after the experiments.

7.3.3 Results and Discussion

The top layer microstructure of the manual metal arc weld deposit was found to contain primary M_7C_3 carbides in the eutectic mixture of austenite and M_7C_3 carbides. The results from microanalysis experiments are shown in Fig. 7.11, and the mean concentrations are summarised in Table 7.3 with a carbon correction as explained in the last section. The experimentally measured partition coefficient of chromium (k_{Cr}, given by the ratio of wt%Cr in M_7C_3 to that in austenite Fig. 7.12) was found to be ≈3.81 indicating that the as-deposited microstructure is configurationally frozen from about 1100°C resulting in a metastable austenitic matrix. It is expected that the austenite should eventually transform to ferrite and more M_7C_3, as is evident from the phase diagrams presented in Fig. 7.4.

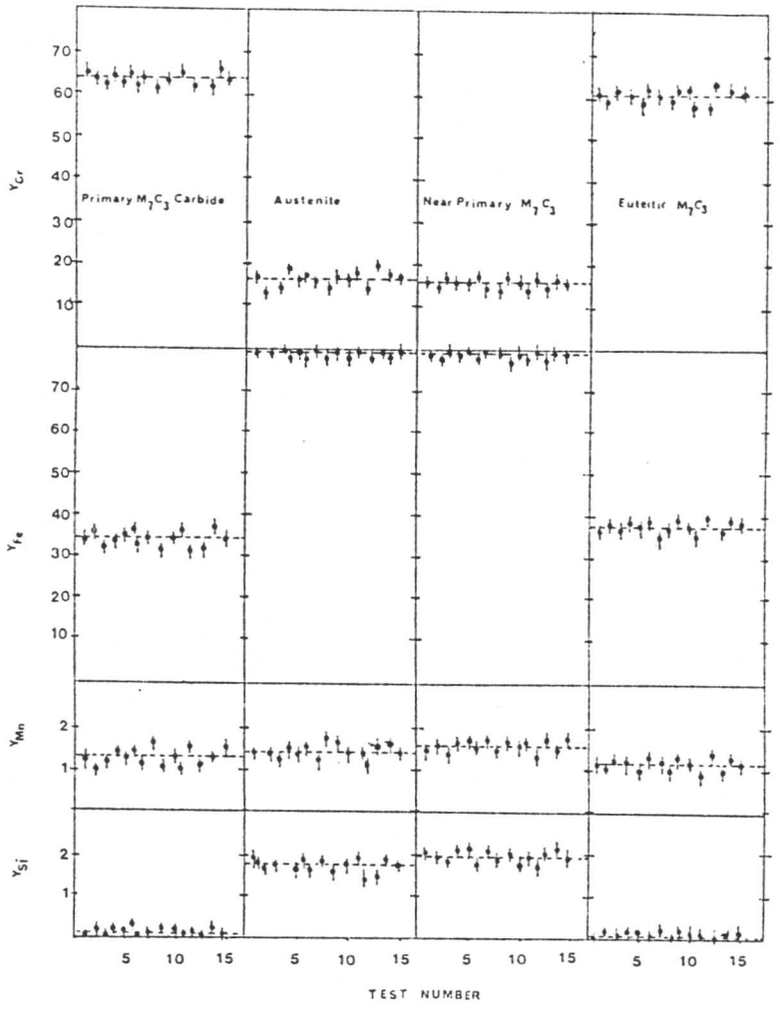

Fig. 7.11: Microanalytical data on primary M_7C_3, eutectic M_7C_3, the austenite near the primary carbides and austenite when the carbon is not included (the continuous lines show the average values in each phase) at%.

Table 7.3: Mean composition of phases. The results are quoted to three decimal places for internal consistency. The results for the primary carbides and the austenite near the primary carbides (Near P. Carbide) are obtained using scanning electron microscopy, whereas the others are determined using transmission electron microscopy.

	Primary Carbide		Near P. Carbide		Austenite		Eutectic Carbide	
	Y_i	V_i	Y_i	V_i	Y_i	V_i	Y_i	V_i
Fe	34.433	24.112	80.794	76.070	80.806	76.080	37.617	26.340
Cr	64.141	44.910	15.636	14.723	16.024	15.088	61.067	42.760
Mn	1.323	0.926	1.588	1.495	1.390	1.308	1.231	0.862
Si	0.103	0.072	1.983	1.864	1.780	1.676	0.085	0.059
C		30		5.840		5.840		30

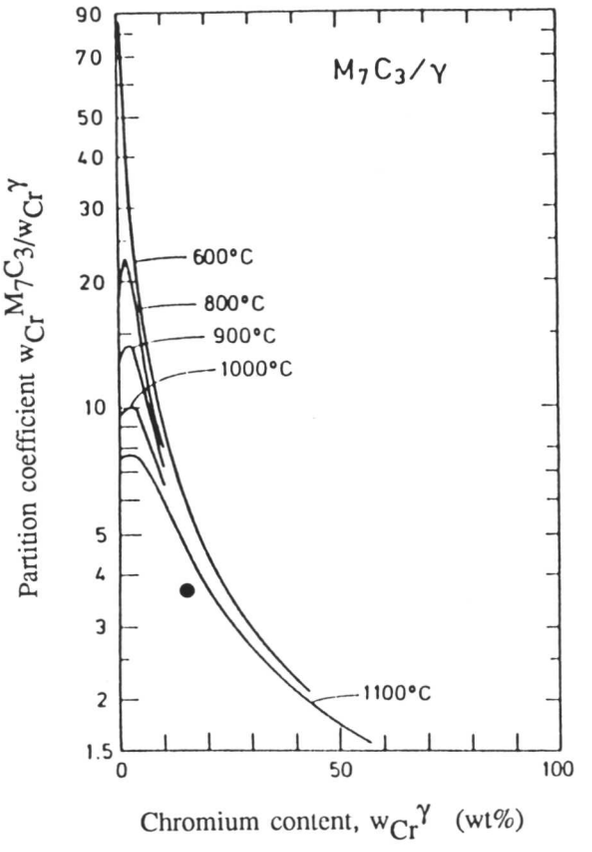

Fig. 7.12: Variation of the partitioning coefficient of chromium as a function of temperature.[7] The point represents the experimental partition coefficient from which it is concluded that the microstructure is configurationally frozen at a temperature above $1100^{o}C$.

In order to understand the nature and kinetics of the transformation of austenite, isothermal dilatometric experiments were carried out at 800, 750, and 700°C. The relative length change versus time curves at three different temperatures are given in Fig. 7.13. The transformation results in a volume contraction and this can be explained theoretically as follows;

$$\frac{\Delta V}{V} = \frac{X_\alpha \frac{N_T}{2} a_\alpha^3 + (X_\gamma - X_\alpha)\frac{N_T}{56} Y_{M_7C_3}^{(2)} + \frac{N_T}{56} X_{M_7C_3} Y_{M_7C_3}^{(1)} - \frac{N_T}{4} X_\gamma a_\gamma^3 - \frac{N_T}{56} X_{M_7C_3} Y_{M_7C_3}^{(1)}}{\frac{N_T}{4} X_\gamma a_\gamma^3 + \frac{N_T}{56} X_{M_7C_3} Y_{M_7C_3}^{(1)}} \quad .....(7)$$

where $\Delta V/V$ is the relative volume contraction as a result of $\gamma+M_7C_3 \rightarrow \alpha+M_7C_3$ transformation,

X_α = mole fraction of metal atoms in ferrite,

N_T = total number of metal atoms,

a_α = lattice parameter of ferrite at the reaction temperature;

$$a_\alpha = \bar{a}_\alpha \; [\, 1 + l_\alpha \, (T-25)] \quad .....(8)$$

$\bar{a}_\alpha$ = lattice parameter of ferrite at the ambient temperature = 2.8633 Å, measured by X-ray diffraction,

l_α = linear expansion coefficient of ferrite (Table 7.4),

T = temperature in °C,

X_γ = mole fraction of metal atoms in austenite,

a_γ = lattice parameter of austenite at the reaction temperature;

$$a_\gamma = \bar{a}_\gamma \; [\, 1 + l_\gamma \, (T-25)] \quad .....(9)$$

$\bar{a}_\gamma$ = lattice parameter of austenite at ambient temperature = 3.620 Å, measured by X-ray diffraction,

l_γ = linear expansion coefficient of austenite = $1.8431 \; 10^{-5}$,[12]

$Y_{M_7C_3}^{(2)}$ = volume of a unit cell of M_7C_3 at the reaction temperature;

$$Y_{M_7C_3}^{(2)} = (3 \; a_{M_7C_3}^2 \; 3^{-1/2} \; c_{M_7C_3}) / 2 \quad .....(10)$$

$a_{M_7C_3}$ = lattice parameter (a) of M_7C_3 carbides at the reaction temperature;

$$a_{M_7C_3} = \bar{a}_{M_7C_3} \; [1 + l_{M_7C_3} \, (T-25)] \quad .....(11)$$

$\bar{a}_{M_7C_3}$ = lattice parameter (a) of M_7C_3 at the ambient temperature = 13.77 Å,

$l_{M_7C_3}$ = linear expansion coefficient of M_7C_3 (Table 7.4),

$c_{M_7C_3}$ = lattice parameter (c) of M_7C_3 carbides at the reaction temperature;

$$c_{M_7C_3} = \bar{c}_{M_7C_3} 3[1 + l_{M_7C_3} \, (T-25)] \quad .....(12)$$

$\bar{c}_{M_7C_3}$ = lattice parameter (c) of M_7C_3 at the ambient temperature = 4.44 Å,

$X_{M_7C_3}$ = mole fraction of metal atoms in M_7C_3,
$Y^{(1)}_{M_7C_3}$ = volume of a unit cell of M_7C_3 before transformation = 2187.27 A^3,
2, 4 and 56 are the number of metal atoms in a unit cell of ferrite, austenite, and M_7C_3 phases respectively.

Equation 8 can be rewritten as;

$$\frac{\Delta V}{V} = \frac{\frac{X_\alpha}{2}a_\alpha^3 + \frac{(X_\gamma - X_\alpha)}{56}Y^{(2)}_{M_7C_3} - \frac{X_\gamma}{4}a_\gamma^3}{\frac{X_\gamma}{4}a_\gamma^3 + \frac{(1-X_\gamma)}{56}Y^{(1)}_{M_7C_3}} \qquad .....(13)$$

and

$$\approx \frac{\frac{V_\alpha}{2}a_\alpha^3 + \frac{(V_\gamma - V_\alpha)}{56}Y^{(2)}_{M_7C_3} - \frac{V_\gamma}{4}a_\gamma^3}{\frac{V_\gamma}{4}a_\gamma^3 + \frac{(1-V_\gamma)}{56}Y^{(1)}_{M_7C_3}} \qquad .....(14)$$

where V_α, and V_γ are volume fractions of ferrite and austenite respectively.

After the transformation of austenite, the volume contraction as a function of the volume fraction of ferrite at 750°C was calculated as outlined above and the results are compared with the experimental observation in Fig. 7.14.

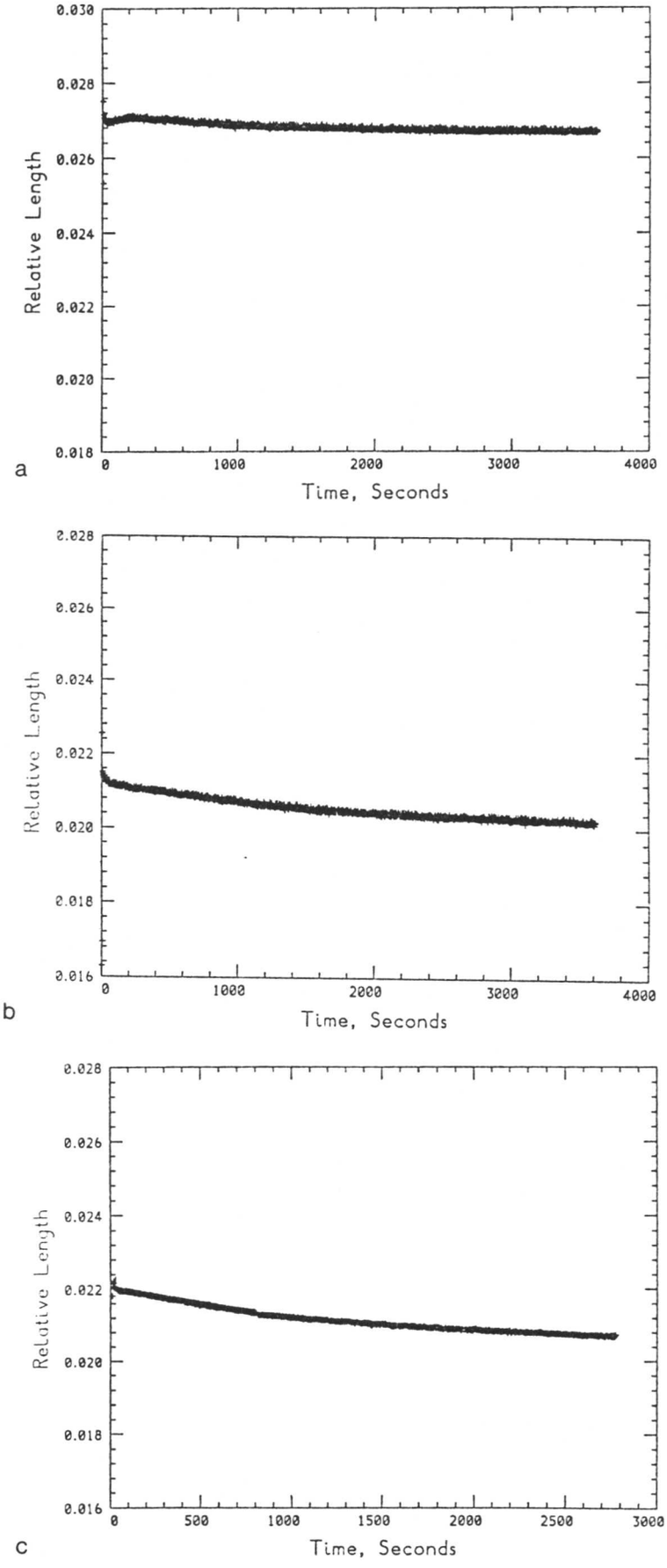

Fig. 7.13: Relative length change versus time curves at a) 700; b) 750; c) 800^{o}C.

Table 7.4: Linear thermal expansion coefficients (10^6, K^{-1}) for ferrite, and M_7C_3phases at a variety of temperatures ^oC. After Ershov.[13]

Temperature	100	200	300	400	500	600	700
Ferrite	12.3	13.3	13.6	14.4	14.8	15.7	16.3
M_7C_3	8.8	10.4	11.8	12.1	13.7	13.8	15.3

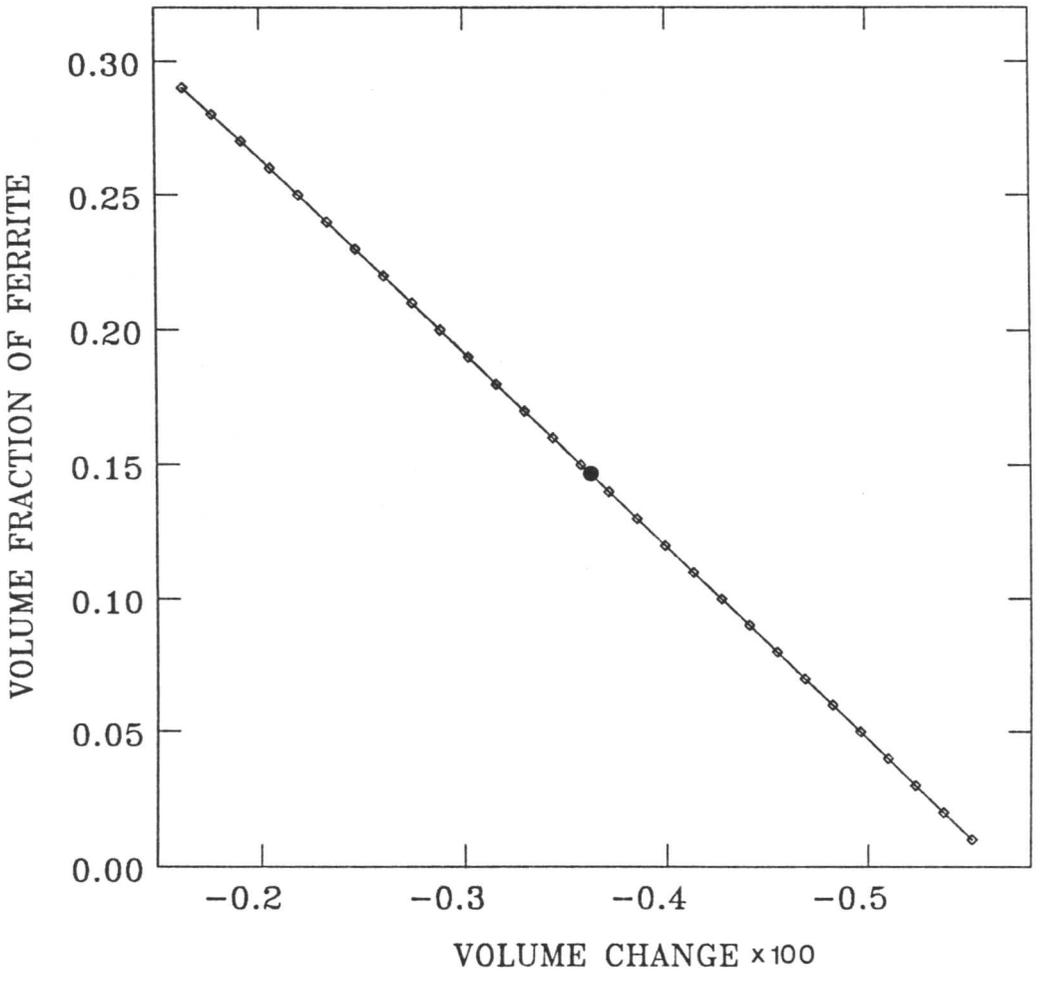

Fig. 7.14: The volume contraction expected as a function of the volume fraction of ferrite at 750^oC when austenite transforms to $M_7C_3+\alpha$. The point (●) marked on the line shows the experimentally observed volume contraction at 750^oC suggesting that the microstructure after about 3500 seconds contains ≈15% ferrite.

Thin foils for transmission electron microscopy were prepared in samples quenched after holding at reaction temperatures for 100, 500, 1000 seconds and 24 hours. After 100 seconds at 750^{o}C, the matrix is found to be austenitic but containing fine carbide particles (Fig. 7.15). These carbides were identified as $M_{23}C_6$ in a cube-cube orientation with the fcc matrix (Fig. 7.15b), as is usually the case with such carbides. The $M_{23}C_6$ carbide is not a thermodynamically stable phase for this alloy (as evident from the isothermal phase diagrams, Fig. 7.4). The nucleation of these carbides could be nevertheless associated with a good match of metal atoms on the interface between the austenite and $M_{23}C_6$ phases. A good match across the interface plane lowers the interfacial energy for nucleation.[15-17] The bright field image of the carbides reveals fringes that probably arise from the displacement associated with the precipitate misfit.[14] These fringes are similar to the stacking faults and this is demonstrated in bright field and dark field images which reveal opposite fringe contrasts (Fig. 7.15a,c).

Besides the nucleation of $M_{23}C_6$ carbides in the matrix, protrusions were observed along the eutectic-M_7C_3/matrix interface (Fig. 7.16). When the {242} $M_{23}C_6$ diffraction spot is used for dark field imaging, these protrusions were illuminated (Fig. 7.16b) suggesting that they are probably $M_{23}C_6$ which nucleated at the carbide/matrix interfaces.

The matrix was found to have transformed to ferrite after 500 seconds. The dark field images (Fig. 7.17a,b) show that two ferrite grains surround the $M_{23}C_6$ carbides. After 24hrs at 750^{o}C, the microstructure revealed the presence of M_7C_3 carbides in the ferritic matrix (Fig. 7.18). This indicates that $M_{23}C_6$ carbides transform to M_7C_3 which is the equilibrium phase. Optical micrographs before and after the transformation are given in Fig. 7.19 to illustrate the effect of this transformation on the microstructure.

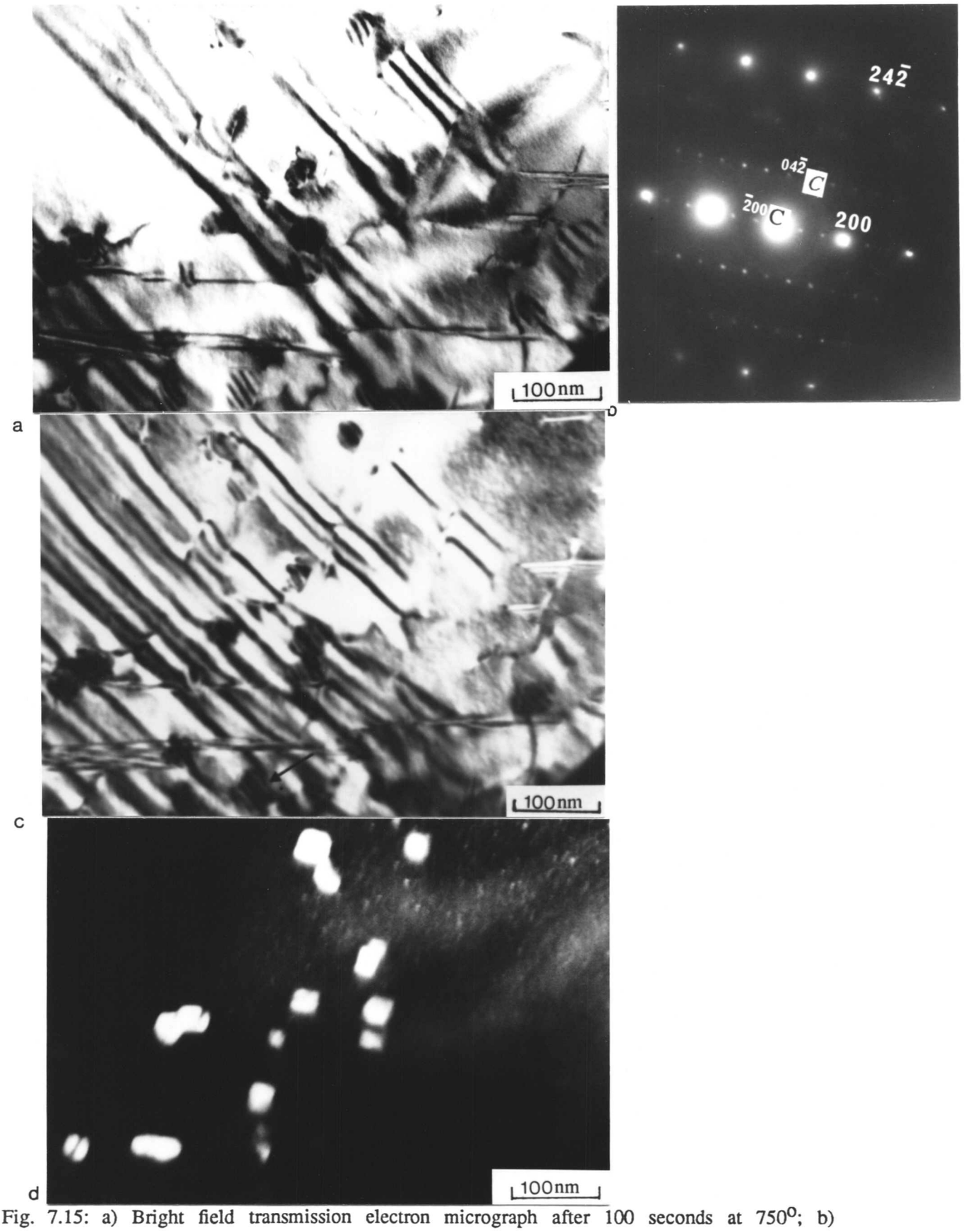

Fig. 7.15: a) Bright field transmission electron micrograph after 100 seconds at 750°; b) corresponding electron diffraction pattern showing $[012]_{\gamma}$ // $[012]_{M_7C_3}$ zone axis with a cube-cube orientation relationship; c) dark field image using {220} matrix reflection the fringes (indicated by the arrow) show opposite contrast compared with the bright field image; d) corresponding dark field image using {242} carbide reflection.

a

b

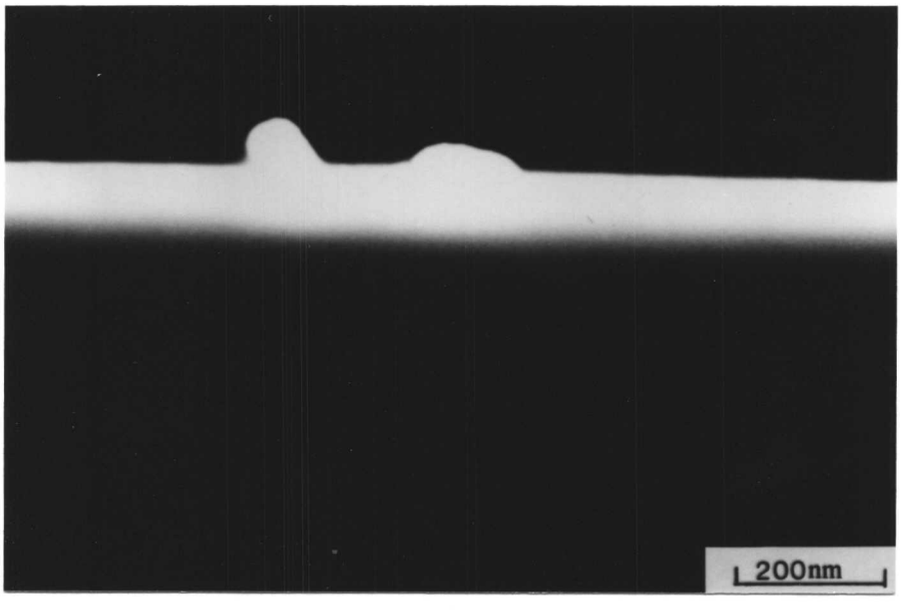

Fig. 7.16: a) Bright field transmission electron micrograph after 100 seconds at 750^{o}C showing a carbide protrusion into the austenite; b) dark field image of the protrusions using a (242) carbide reflection.

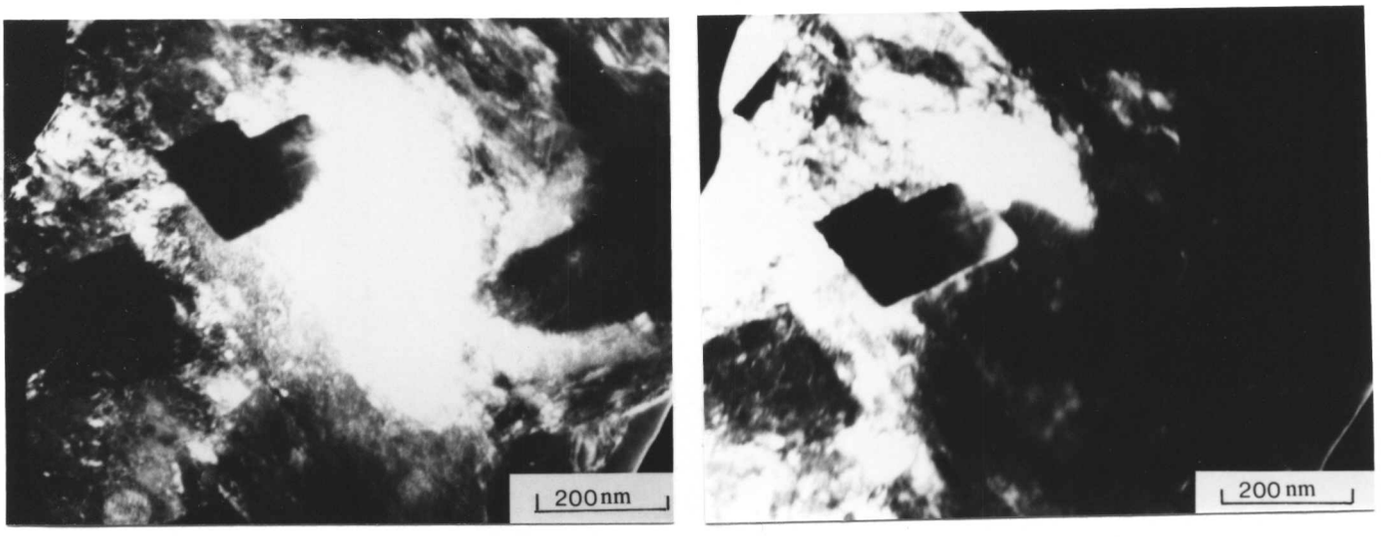

a b

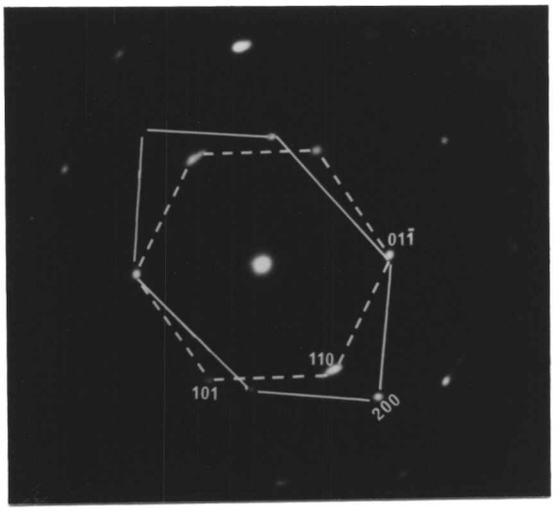

c

Fig. 7.17: Dark field images from ferrite grains, a) using a $(110)_\alpha$ reflection; b) using a $(200)_\alpha$ reflection; c) corresponding electron diffraction pattern showing two ferrite patterns.

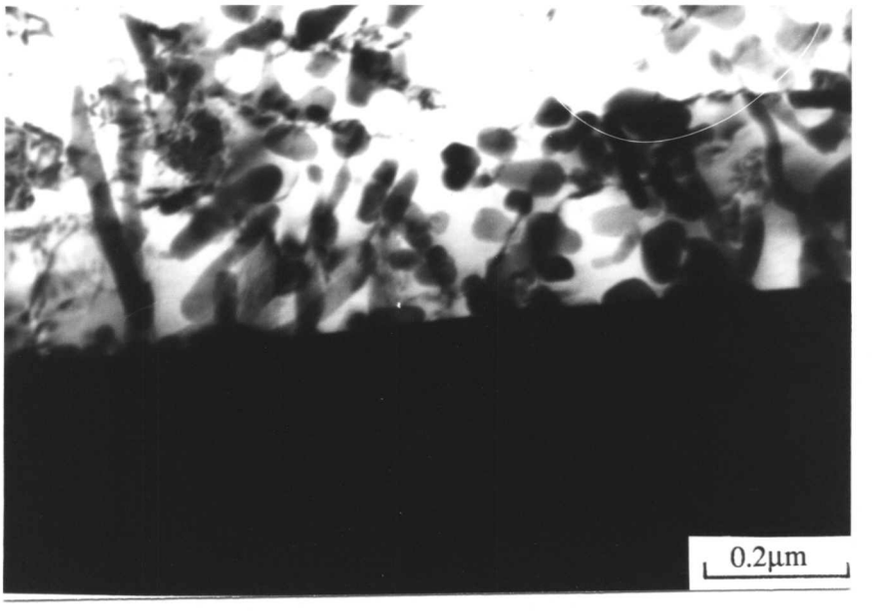

a

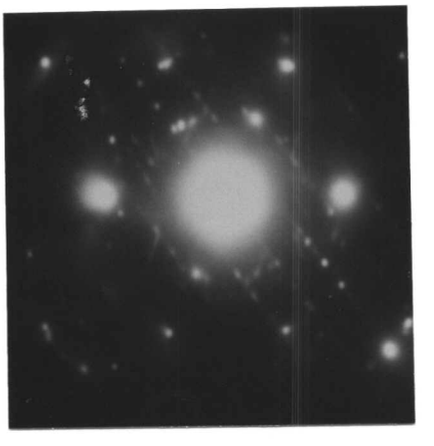

b

Fig. 7.18: a) Bright field transmission electron micrograph after 24hrs. at 750°C showing the transformation products of ferrite and M_7C_3 carbides; b) corresponding electron diffraction pattern, showing $<012>_{\alpha}$ // $<10.0>_{M_7C_3}$ orientation relationship.

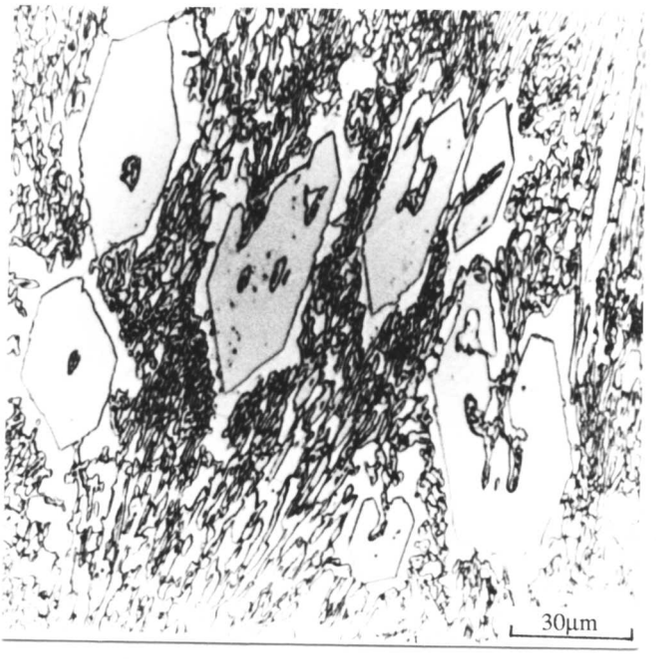

a

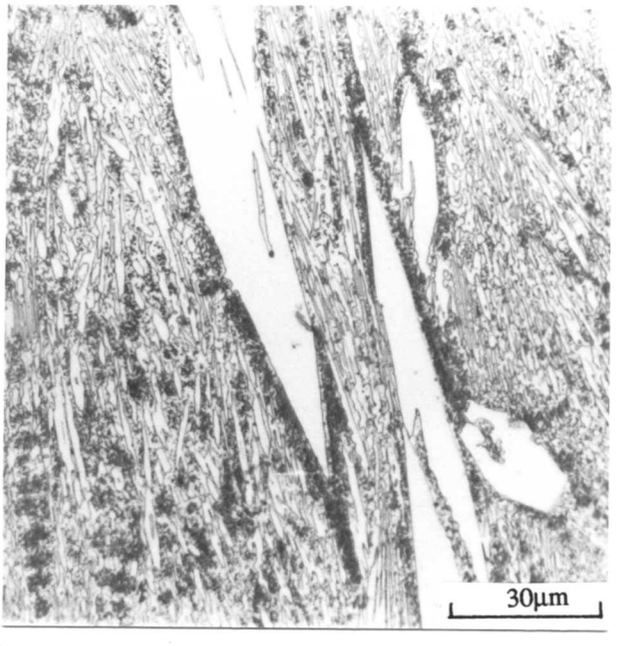

b

Fig. 7.19: Optical micrographs, a) before the transformation; b) following transformation of austenite (after 24hrs. at 750^{o}C). Note the change in etching contrast.

7.4 Conclusions

Fe-29.19Cr-3.80C-1.31Mn-0.59Si-0.01Mo (wt%) hardfacing alloy deposited by the manual metal arc welding technique has a metastable austenitic matrix. The austenite tends to transform to ferrite and M_7C_3 carbides as evident from the equilibrium isothermal phase diagrams below 850°C. The kinetics of this transformation were studied at 700, 750, and 800°C. The results showed that $M_{23}C_6$ carbides form in the austenitic matrix. This carbide is not a thermodynamically stable phase but forms because it is able to nucleate more easily with a cube-cube orientation relationship with the austenite. A good match on the interface lowers the interfacial energy and promotes the nucleation of the $M_{23}C_6$ carbides. As the reaction goes on, the austenite transforms to ferrite which engulfs the $M_{23}C_6$ carbides, since they are in regions which are depleted in carbon and chromium. The matrix was found to be completely ferritic with M_7C_3 carbides after 24 hours indicating that $M_{23}C_6$ carbides eventually transform to M_7C_3 which is the equilibrium phase. The dilatometric results are discussed on the basis of theoretical calculations and an agreement was found reasonably well.

7.5 Effect of Mn and Ni on the Microstructure and Abrasive Wear Resistance

7.5.1 Introduction

The microstructure of the Alloy 78, as deposited by the MMA welding technique, is metastable and given sufficient thermal activation tends to equilibrate. Equilibration involves the decomposition of austenite into ferrite and M_7C_3 carbides at temperatures around 700^{o}C. As discussed in the previous section the experimental results showed that this reaction is quite fast, even though it involves long-range substitutional atom diffusion. Also, the diffusional transformation of austenite leads to a ferrite matrix with a decreased Cr concentration, suggesting an inevitable decrease in oxidation and corrosion resistance. Therefore, the matrix must be modified. It is known that Mn and Ni are strong austenite stabilizing elements so that they enlarge the austenite field in Fe-C phase diagram. Hence, attempts have been made to stabilise the austenitic matrix of the Alloy 78 with the addition of Mn and Ni. These alloying elements are generally added to the Fe-based hardfacing alloys in order to stabilise the austenite in a matrix, and to reduce the tendency to crack on cooling in welding processes.[18] Mn is more commonly added to hardfacing steels rather than high Cr irons. For instance, up to 15wt% Mn is added to high chromium austenitic steels to stabilise the austenite and up to 5wt% Mn could be present in martensitic steels to aid weldability.[19] High strength is achieved in the Mn containing steels which have been developed due to their high strain hardening character. Strain induced austenite-martensite transformation and/or twinning give rise to an increase in the work hardening characteristics of these alloys.[20]

As far as the abrasive wear resistance is concerned, austenitic alloys which are capable of transforming to strain-induced martensite show excellent wear resistance. In austempered spherical cast irons,[21] in high Mn steels,[20] and in tool steels[22] very good abrasive wear resistance is achieved as a result of strain-induced-martensite formation. It is suggested that the volume increase as a consequence of martensitic transformation retards the formation of microcracks, and subsequently leads to better wear resistance. Furthermore, it is believed that high surface hardness due to work hardening significantly reduces weight loss. The beneficial effect of stabilising the austenite in the matrix has been demonstrated in industrial applications. For instance, popet valves, which are usually hardfaced by Co-based hardfacing alloys have been replaced by the Fe-based alloy (Fe-28Cr-15Ni-(5.5Mo+W/2)-2.0C wt%) which contains 15wt% Ni.[23] In this alloy a high amount of Ni provides excellent weldability, and also stabilises the austenitic matrix, which is believed to have a higher degree of wear resistance than ferritic matrix. The austenitic matrix is also strengthened with high interstitial levels of nitrogen with either Mn, or Ni. In a wide range of work hardenable steels, the highest work hardening rate was reported in nitrogen strengthened alloys.[20]

Mn and Ni also have a beneficial effect on oxidation and corrosion resistance of high Cr irons. For example, Ni is widely added to austenitic cast irons in corrosive conditions because it forms a protective corrosion resistant film on the surface of the material.[24] Ni-Cr white alloy,